Nonlinear Model Predictive Control for Path Following of Autonomous Inland Vessels in Confined Waterways

Chengqian Zhang[a], Abhishek Dhyani[b*], Jonas W. Ringsberg[a], Fabian Thies[a], Rudy R. Negenborn[b], Vasso Reppa[b]

[a] *Department of Mechanics and Maritime Sciences, Division of Marine Technology, Chalmers University of Technology, SE-412 96 Gothenburg, Sweden*

[b] *Department of Maritime and Transport Technology, Delft University of Technology, Mekelweg 2, 2628 CD, Delft, The Netherlands*

Abstract

Autonomous inland shipping offers a safer and more efficient form of transportation over water with the potential to reduce maritime carbon emissions. However, the operation of autonomous vessels presents unique challenges due to complex dynamics, varying traffic conditions, and environmental disturbances. To ensure the safe navigation of these vessels in confined inland waterways, it is crucial to address manoeuvring prediction and motion control challenges. Research focusing on these challenges disregards or only partially incorporates inland waterway characteristics related to the vessel and its surroundings. This study provides a comprehensive analysis of these key factors. By modelling the vessel using a modified Manoeuvring Modelling Group (MMG) model specifically tailored for confined waterways, hydrodynamic effects due to shallow water, channel banks, and current are accounted for. A nonlinear model predictive controller (NMPC) is employed for the vessel path following control under various scenarios, including straight channels, confluences, and river bends. It is observed that the hydrodynamic effects from the channel banks significantly impact vessel steering. Compared to conventional proportional-integral-derivative (PID) controllers, NMPC effectively reduces course deviations and cross-track errors under varying water depth and ship-to-bank distance conditions, while also requiring fewer rudder deflections. Furthermore, key performance metrics related to the control of inland waterway vessels are proposed to evaluate the controller's performance further. The NMPC control law demonstrates its effectiveness in capturing the hydrodynamic effects and improving navigation safety in confined waterways.

1. Introduction

The European inland waterways, which extend over 41,000 kilometres of rivers and canals, form a complex transport network connecting 25 countries, numerous cities, and vital industrial regions. Despite their extensive network, these waterways have been underutilised in the past decade, accounting only for 6% of the continent's inland freight transport, in contrast to the 77% dominated by road transport (European Commission, 2023). Given the strict emission regulations and road congestion issues within the European Union, enhancing the use of inland waterways could be a reliable and effective solution.

Autonomous shipping has emerged as a popular research topic within the maritime community due to its potential to improve navigational safety, enhance traffic flow with optimal energy efficiency and reduce operational costs. With the development of sophisticated sensors, algorithms, and intelligent navigation systems, autonomous vessels offer improved situational awareness. This is particularly interesting for inland shipping, where vessels navigate in complex environments and within narrow waterway boundaries. By using advanced automation systems onboard, autonomous inland waterway vessels (IWVs) can handle challenging scenarios such as path planning and collision avoidance, thereby contributing to a reliable and safe inland waterway transport network.

Given that inland waterways have distinct navigation environments as compared to open water, various technological and legislative challenges must be considered to support the development and deployment of autonomous IWVs in confined waters. This requires a thorough examination of the vessel's design, perception, path planning, motion control, and potential socio-technical challenges (European Commission, 2020). Among these elements, providing an energy-efficient route, or voyage planning, stands out as a crucial challenge to ensure that these vessels meet environmental sustainability goals. To accomplish this, it is critical to establish a comprehensive system that can reflect and optimise energy management throughout the dynamic operations of vessels. This system should include a ship energy performance model (Zhang et al., 2023), a manoeuvring model, control design, and routing algorithms. This work aims to tackle the challenges associated with manoeuvring and effective control of IWVs, which are vital elements in the operational analysis of dynamic inland waterways.

Operating IWVs in confined waters is challenging as they are constrained by factors such as canal width, infrastructure, dynamic water levels, river currents and riverbed variations. Water depth, especially the impact of shallow waters, significantly affects a vessel's motion and manoeuvrability (Du et al., 2020; Kijima and Nakiri, 1990; Liu et al., 2015; Mucha et al., 2019; Pompée, 2015; Yoshimura, 1986). Furthermore, IWVs must frequently sail close to one side of the bank to clear the way for other upcoming or passing vessels, making the vessel approach the channel wall. This can result in flow acceleration between the gap, generating additional hydrodynamic forces on the hull, which poses challenges to vessel steering and handling, the so-called bank effect (Lee and Lee, 2008; Vantorre et al., 2003). Shallow water and bank effects are suspected as factors responsible for several grounding accidents, including the infamous 2021 Suez Canal obstruction (BBC News, 2021). Therefore, a precise and robust mathematical model is critically important to ensure the operational safety of these full-scale autonomous vessels, as it helps predict the vessel's motion response on confined water under these hydrodynamic effects. In addition, effective control techniques must be developed to safely and precisely follow the desired track while using the minimum effort from the propulsion and steering system. By reducing unnecessary manoeuvres and optimising the steering commands, the vessel can mitigate the wear and tear on the whole system and lead to less energy consumption, which is essential to, e.g., an electrified vessel for maintaining the vessel's operational efficiency over longer distances without frequent recharging.

1.1. Vessel manoeuvring modelling

Vessel manoeuvring is a critical research topic that has been continuously developed during the past decades. The existing studies on manoeuvring can be classified into two categories: (i) free running tests, by directly conducting model tests and full-scale trails with acting propeller and rudder to analyse the vessel's steering ability; (ii) mathematical model-based methods, focusing on solving equations of vessel's motion as rigid body dynamics to update its states based on the speed and rudder input. Due to the high cost of free-running experiments and difficulties in providing manoeuvring predictions of vessels under construction, most research has been conducted based on mathematical manoeuvring models, which can generate fast and accurate movement predictions. Some typical manoeuvring models, such as the linear Nomoto model and those nonlinear models (Abkowitz, 1964; Nomoto et al., 1957; Ogawa and Kasai, 1978) have been widely used in maritime society based on various application demands and purposes. Nevertheless, these models are developed for open water applications by using

the profile of classical commercial vessels, reducing their applicability to inland waterways where vessels must navigate in shallow and confined waterways most of the time. Research on the shallow water effect on manoeuvring has been conducted continuously for decades. Kijima and Nakiri (1990) proposed the famous MMG-based model for hydrodynamic derivatives corrections in shallow water. These semi-empirical formulas were derived using model tests and lifting surface theory from classical seagoing vessels. Yoshimura (1986) used the MMG model for manoeuvring prediction of a car carrier under various water depth conditions. The simulation results show good agreement with the experimental data, but also emphasise the shortcomings of calculated hydrodynamic coefficients as they are vessel-specific, meaning that the application on IWVs reduces since the hull types might differ significantly. In addition to model tests, several researchers (Kaidi et al., 2017; Kim et al., 2022; Mucha, 2017; Okuda et al., 2022) used computational fluid dynamics (CFD) to quantify the impact of shallow water on vessel manoeuvring, but the focus was still on an individual vessel type by correcting the hydrodynamic coefficients rather than proposing a generic manoeuvring model. Liu et al. (2017b) proposed a holistic manoeuvring model, especially for inland vessels on the Yangtze River in China. This model uses the well-known manoeuvring modelling group (MMG) model as the baseline with specific modifications for twin propeller inland vessels, including a rudder modelling using two-dimensional CFD simulation. However, the study focused only on navigation on the Yangtze River, which has a larger water depth and wider channel width than European inland waterways, meaning that the water depth or other confinement effects were neglected.

From existing literature, it can be concluded that to enhance the accuracy of predictions concerning the dynamics of IWVs, a suitable manoeuvring model must be derived and applied to confined water scenarios. One of the related works was conducted by Yang and el Moctar (2024). By using massive captive model tests at varying water depths, a new Abkowitz-type model was developed, including the shallow water effect on manoeuvring forces and moments, and the results were successfully validated against experimental and full-scale trials of an inland vessel. In a different perspective, Zhang et al. (2024b) proposed a modified MMG model by incorporating additional terms of bank effect; the shallow water effect was modelled with hydrodynamic derivatives under various water depths. The model was validated using turning test data of a pusher-barge model (Koh and Yasukawa, 2012). A rudder control scheme was subsequently developed, followed by a course-keeping analysis that included these shallow water, bank, and current effects. However, the simulation was limited to straight waterways, and the heading control was relatively simplistic, suitable only for navigating straight courses.

1.2. Vessel path-following control

In addition to vessel manoeuvring modelling, research efforts to enhance vessel motion control have also been witnessed during the past decade, focusing on the vessel path-following problem. Path-following control system design can further be categorised into linear path-following or course-keeping, which involves controlling the vessel to maintain a straight-line trajectory, and curved path-following, involving intricate steering mechanisms to navigate the bends in the pathway. Curved path following is a comparatively complex task due to the need to counteract the vessel's lateral drift, which primarily results from its inertia and hydrodynamic disturbances (Wang et al., 2019). To account for the modelling uncertainties and limited knowledge of the environmental forces such as wind and currents, a robust control law must be designed to counteract their effect on the vessel; see, for example, (Chen et al., 2023; Paulig and Okhrin, 2024; Sun et al., 2017; Xu et al., 2023). Model-based robust control algorithms

aim at estimating and eliminating the impact of these disturbances on vessel navigation, applying techniques such as active disturbance-rejection (Sun et al., 2017), neural networks (Park et al., 2017; Wei et al., 2017), model-predictive control (Fu et al., 2023; Zheng et al., 2016), feedback linearisation (Chen et al., 2023), reinforcement learning (Hart et al., 2023; Waltz et al., 2025), and sliding-mode control (Zhang et al., 2020a), to name a few. However, most of these proposed methods only focus on the environmental disturbances dominating the open sea environment while maintaining sea-going vessel characteristics (single-propeller, single-rudder designs). This is because modelling the inland waterway characteristics (bank and shallow-water effects) using physical laws was lacking in the existing literature. As a result, these algorithms are inadequate in providing good control performance in inland waterway conditions. Motion control in restricted waterways such as rivers and port areas has recently been a focus in some works (Du et al., 2022a; Xu et al., 2023); but requires further research on control design.

Navigating in inland waterways introduces additional constraints, such as the bank effect and shallow-water effect, which can significantly impact the performance of traditional controllers (Chen et al., 2021; Sano et al., 2014), making the control synthesis problem more complex. Current maritime navigation systems, such as track pilots, are often based on a Proportional-Integral-Derivative (PID) control law or its variants due to their simplicity and ease of implementation (Alessandri et al., 2015; Zhang et al., 2020b). In a previous work by the authors (Zhang et al., 2024a), a PID control algorithm was proposed for the modified MMG model proposed in (Zhang et al., 2024b) for the vessel path following under various course-keeping as well as steering scenarios. However, the performance and robustness of the proposed algorithm in river confluences and under the presence of river currents were insufficient, as large cross-track errors were still observed. This was partly due to the nonlinear effects, which are more significant during complex manoeuvres and could not be counteracted by the model-free PID controller. Furthermore, the performance analysis of the control design was absent. Finally, the waterways were modelled to have a rectangular-shaped cross-section and a constant water depth, meaning that the impact of bank geometry was neglected and thus failed to fully represent a real inland waterway. It was concluded that these factors necessitate the development of sophisticated model-based control algorithms to ensure safe navigation.

Model Predictive Control (MPC) has been a widely popular control technique for the path-following control design of ASVs (Fu et al., 2023; Li et al., 2020; Zheng et al., 2014). By employing a prediction model, MPC is capable of predicting and accommodating changes in the system's future behaviour. This makes it an attractive choice for vessel navigation applications, where proactive decision-making is crucial due to the vessel's large inertia and limited manoeuvrability. Furthermore, MPC can explicitly take into account the constraints on the vessel inputs and states, facilitating the constrained control requirements of inland navigation. Since the performance of the MPC algorithm greatly relies on the model's accuracy, a detailed manoeuvring model is a foremost requirement for control design. Many existing works have addressed the path-following control problem for autonomous vessels using linear MPC (Haseltalab and Negenborn, 2019; Zhang et al., 2017; Zheng et al., 2014; Zheng et al., 2016). These methods use models obtained by successive linearization around the operation point, which may change significantly. However, a wide range of operating conditions (e.g., varying water depths, variable proximity to channel wall, sharp turns) cannot be effectively represented by a single linear manoeuvring model around a fixed point. As a result, for large prediction times, this will lead to a

significant model mismatch and therefore, large tracking errors (Zheng et al., 2014). Unlike open-sea navigation, where ample space allows for gradual course corrections, the confined and dynamic nature of inland waterways demands high-fidelity modelling of the aforementioned effects to ensure safe navigation. Nonlinear MPC (NMPC) utilizes the complete model of the vessel, ensuring that various nonlinear effects, as well as the varying operating conditions in the inland waterways, can be accounted. However, NMPC is known to have a high computational burden, which may lead to implementation issues, as the underlying optimization problem may not timely converge. Several methods have been proposed in the literature to address this issue, such as using explicit MPC (Tondel et al., 2003), direct multiple shooting (Kirches et al., 2012), real-time iteration (Gros et al., 2020), etc. The direct multiple-shooting method has also been employed for vessel path-tracking control applications, see (Abdelaal et al., 2018; Kayacan et al., 2019; Kosch et al., 2021).

1.3. Contributions of the paper

The main contribution of this work is two-fold. Firstly, we propose the design of an NMPC control law for the path following control of the IWV. The dynamics of the IWV are modelled using an improved manoeuvring simulation model, designed specifically for inland waterways based on physical laws to effectively capture the unique hydrodynamic effects. The vessel's trajectories are modelled using a modified MMG model (Zhang et al., 2024b) and include environmental factors such as water depths, river currents, and bank effects. This further facilitates the simulation and analysis of a virtual autonomous vessel's steering performance in confined waterways. To address the high computational time issue, the NMPC optimization problem is implemented using a direct multiple-shooting method. This method reduces the propagation of the nonlinearity within the optimal control problem (OCP) formulation, leading to a faster convergence of the NMPC optimization problem. As a result, the computational time required is significantly reduced. Secondly, an extensive case study is performed considering a pusher-barge model to validate the performance of the proposed control design in diverse and complex inland waterway situations, such as navigating river bends and intersections. New key performance metrics are proposed for evaluating the performance of the controlled operation on inland waterways. The vessel's steering capabilities are further compared against a standard model-free control technique based on a PID control law, as it represents an industry benchmark at present. The comparative analysis highlights the proposed control law's superior performance and robustness to external disturbances.

2. Methodology

This section describes the major methods and assumptions used in the work. The subsection 2.1 introduces the modified MMG model and highlights modified terms regarding the hydrodynamic effect of confined water, subsection 2.2 showcases the schematics of control design, and various control algorithms.

2.1. Manoeuvring model in inland waterway

The manoeuvring model follows the architecture in Zhang et al. (2024b), where the effect of shallow water was modelled by two parts: (i) increasing resistance, especially the viscous pressure coefficient, is predicted using the methods from Zhang et al. (2023), and (ii) surge force and moments during steering in shallow water were calculated straightforwardly using hydrodynamic derivatives from the experiment. In addition, the bank effect is a critical factor for navigation in narrow fairways, which is

calculated using the method from Vantorre et al. (2003), where the lateral force and the yaw moment are modelled based on the vessel-bank distance, the water depth, and the bank geometry.

2.1.1. Equations of motion

IWVs typically operate at a steady, low speed and therefore do not frequently encounter high waves or strong winds. Consequently, the manoeuvring model in this study focuses on two-dimensional (2D) planar ship motion with three degrees of freedom (3-DoF), considering only surge, sway, and yaw motions, as illustrated in Figure 1. The earth-fixed coordinate system is denoted by $o_0 - x_0 y_0 z_0$, while $o - xyz$ represents the body-fixed coordinate system of the inland vessel, with the origin located at the midship. The midship position is defined at the geometrical centre of the vessel. The vessel heading (ψ) is defined as the angle between the $o_0 - x_0$ axis and the $o - x$ axis, and the rudder angle is represented by δ. The coordinates of the centre of gravity (x_G, y_G) are expressed in the earth-fixed coordinate system as (x_{0G}, y_{0G}).

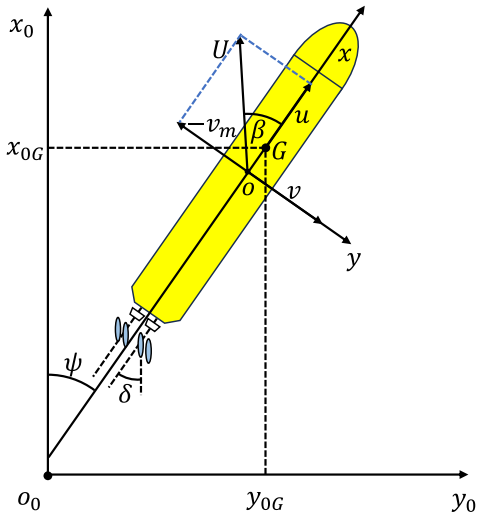

Figure 1. Coordinate system of an IWV.

The equations of rigid body dynamics for IWVs operating in restricted water are represented as:

$$\left.\begin{aligned}(m+m_x)\dot{u} - \left(m + m_y\right)v_m r - x_G m r^2 &= X_H + X_P + X_R + X_B \\ (m+m_x)\dot{v}_m - (m+m_x)ur + x_G m\dot{r} &= Y_H + Y_R + Y_B \\ (I_z+x_G^2 m+J_Z)\dot{r} + x_G m(\dot{v}_m+ur) &= N_H + N_R + N_B\end{aligned}\right\} \quad (1)$$

where, m is the mass of IWV, m_x and m_y represent the added mass in longitudinal and transverse directions, u is the surge velocity, v_m is the sway velocity at midship, r is the yaw velocity, x_G is the location of the centre of gravity (CoG), I_z is the moment of inertia, and J_Z is the added moment of inertia. The right-hand side is the summation of the surge force X, sway force Y, and yaw moment N, and the subscripts H, P, R, and B represent the individual effect from the hull, propeller, rudder, and bank effect, respectively.

2.1.2. Hydrodynamic force on vessel hull

Hydrodynamic forces on the vessel hull are dimensionless according to the following equation:

$$\left.\begin{aligned} X_H/(0.5\rho LTU^2) &= -R_0' + X_{\beta\beta}'\beta_m^2 + X_{\beta r}'\beta_m r' + X_{rr}'r'^2 + X_{\beta\beta\beta\beta}'\beta_m^4 \\ Y_H/(0.5\rho LTU^2) &= Y_\beta'\beta_m + Y_r'r' + Y_{\beta\beta\beta}'\beta_m^3 + Y_{\beta\beta r}'\beta_m^2 r' + Y_{\beta rr}'\beta_m r'^2 + Y_{rrr}'r'^3 \\ N_H/(0.5\rho L^2TU^2) &= N_\beta'\beta_m + N_r'r' + N_{\beta\beta\beta}'\beta_m^3 + N_{\beta\beta r}'\beta_m^2 r' + N_{\beta rr}'\beta_m r'^2 + N_{rrr}'r'^3 \end{aligned}\right\} \quad (2)$$

where ρ is the freshwater density, L is the vessel length, T is the draught, and U is the vessel's total speed, R_0' is the resistance coefficient in shallow water (Zhang et al., 2023), β_m is the drift angle at midship, if there is no current, this is calculated by $\beta_m = -tan^{-1}(v_m/u)$, $X_{\beta\beta}'$, $X_{\beta r}'$, …, N_{rrr}' are the so-called hydrodynamic derivatives by regression analysis from the captive model test, r' is the non-dimensional yaw speed ($r' = rL/U$). It should be noted that u, v_m must be modified based on the speed and direction of the water flow if the current effect is included.

2.1.3. Propeller thrust

IWVs are normally equipped with twin propellers. The total longitudinal force delivered from a twin-propeller configuration can be expressed by:

$$X_P = (1-t)\left(T_P^P + T_P^S\right) \quad (3)$$

where t is the thrust deduction factor, T_P^P and T_P^S represent the thrust generated from the portside and starboard propeller, which is computed as:

$$T_P^P = T_P^S = \rho n_P^2 D_P^4 K_T(J) \quad (4)$$

In Eq. (4), n_P is the propeller revolution speed, D_P is the propeller diameter, and $K_T(J)$ is the function of the thrust coefficient derived from the open water test under various advanced ratios J:

$$J = u(1-w_P)/(n_P D_P) \quad (5)$$

In Eq. (5), u is the surge velocity, w_P is wake fraction at the propeller in manoeuvring, computed as:

$$w_P/w_{P0} = \exp(-4\beta_P^2) \quad (6)$$

where w_{P0} is the effective wake in a straight motion, β_P is the inflow angle at the propeller, including the drift angle β_m and yaw speed r', given as:

$$\beta_P = \beta_m - (x_P/L)\, r' \quad (7)$$

In Eq. (7), x_P is the position of a propeller in the longitudinal direction. The propulsive coefficients, such as thrust deduction t and wake fraction w_{P0} are regarded as identical for each propeller. This is because of the challenge of analysing the unsymmetrical inflow fields during motions in manoeuvring; the crossflow can alter the wake field, and oblique movement might result in more complicated interactions. To understand this requires sophisticated experimental measurements (Friedhoff et al., 2019) such as Particle Image Velocimetry (PIV) or heavy CFD simulations, which are beyond the scope of the present work.

2.1.4. Rudder steering force and moment

Rudder steering force is a crucial factor as it directly influences the vessel's manoeuvrability. IWVs are normally equipped with twin or multiple rudders for better steering ability. In this work, the rudder forces are computed by:

$$\left.\begin{aligned} X_R &= -(1-t_R)\left(F_N^P+F_N^S\right)\sin\delta \\ Y_R &= -(1+\alpha_H)\left(F_N^P+F_N^S\right)\cos\delta \\ N_R &= -(x_R+\alpha_H x_H)\left(F_N^P+F_N^S\right)\cos\delta \end{aligned}\right\} \quad (8)$$

where t_R is the empirical correction factor to rudder surge force during steering (Yasukawa and Yoshimura, 2015); F_N^P and F_N^S denotes the rudder normal force on the port side and starboard, respectively; δ represents the rudder angle; α_H is the rudder force increase factor; x_R is the relative position of rudders in the longitudinal direction, and x_H is the position where additional lateral force is acting. Like propeller force calculation, the interaction of multiple rudders was neglected in this work, meaning that the rudder normal force is assumed to be identical with the same inflow angle; the equation is given as:

$$F_N = 0.5\rho A_R U_R^2 \left(\frac{6.13\Lambda}{\Lambda+2.25}\sin\alpha_R\right) \quad (9)$$

where A_R is the rudder area, U_R is the resultant inflow velocity at the rudder ($U_R = \sqrt{u_R^2 + v_R^2}$), Λ is the rudder aspect ratio, and α_R is the effective inflow angle at the rudder given by:

$$\alpha_R = \delta - \tan^{-1}\left(\frac{v_R}{u_R}\right) \quad (10)$$

In Eq. (10), u_R and v_R represent the longitudinal rudder inflow velocity and the transverse rudder inflow velocity, respectively. These individual velocities are computed using the equation:

$$\begin{aligned} v_R &= U\gamma_R(\beta - l_R' r') \\ u_R &= \frac{\varepsilon u_P}{1-s}\sqrt{1-2(1-\eta\kappa)s+\{1-\eta\kappa(2-\kappa)\}s^2} \end{aligned} \quad (11)$$

where γ_R is the flow straightening coefficient, l_R' is a constant derived from experiments which denotes the acting point of v_R, s is the propeller slip ratio, η is a ratio of propeller diameter to rudder span ($\eta = D_P/B_R$), κ is a constant from the experiment, and ε is the ratio of wake at the rudder to the wake fraction at the propeller given as:

$$\varepsilon = (1-w_R)/(1-w_P) \quad (12)$$

2.1.5. Bank-induced effect

The bank effect is another important factor that affects vessel handling in inland waterways. In this work, the hydrodynamic forces and bow-out moment are calculated through the methods from Vantorre et al. (2003). A key feature of their mathematical model is that it also decomposes bank-induced force and moment into individual components, which can be easily incorporated into the MMG model:

$$\left.\begin{aligned} Y_B^H &= 0.5\rho LTu^2 \sum_{i=1}^{2}\sum_{k=0}^{2} a_{ik}^H y_B^i \left(\frac{T}{H-T}\right)^k \\ N_B^H &= 0.5\rho L^2 Tu^2 \sum_{i=1}^{2}\sum_{k=0}^{2} \beta_{ik}^H y_B^i \left(\frac{T}{H-T}\right)^k \\ Y_B^P &= 0.5\rho LTV_T^2 \sum_{i=1}^{2}\sum_{k=0}^{2} a_{ik}^P y_B^i \left(\frac{T}{H-T}\right)^k \\ N_B^P &= 0.5\rho L^2 TV_T^2 \sum_{i=1}^{2}\sum_{k=0}^{2} \beta_{ik}^P y_B^i \left(\frac{T}{H-T}\right)^k \\ Y_B^{HP} &= 0.5\rho LTV_T^2 Fr \sum_{i=1}^{2}\sum_{k=0}^{2} a_{ik}^{HP} y_{B3}^i \left(\frac{T}{H-T}\right)^k \\ N_B^{HP} &= 0.5\rho L^2 TV_T^2 Fr \sum_{i=1}^{2}\sum_{k=0}^{2} \beta_{ik}^{HP} y_{B3}^i \left(\frac{T}{H-T}\right)^k \end{aligned}\right\} \quad (13)$$

where Y represents lateral force, N is the yaw moment, the superscripts H, P, HP denote the individual effects of speed (hull), propulsion, and the coupled effect. The term V_T is the reference velocity, Fr is the Froude number, α_{ik}^H, β_{ik}^H, α_{ik}^P, β_{ik}^P, α_{ik}^{HP}, and β_{ik}^{HP} are coefficients from regression analysis, y_B and y_{B3} represent non-dimensional quantities of vessel-bank distance, given as:

$$\begin{aligned} y_B &= \frac{1}{2}B\left(\frac{1}{y_p}+\frac{1}{y_s}\right) \\ y_{B3} &= \frac{1}{2}B\left(\frac{1}{y_{p3}}+\frac{1}{y_{s3}}\right) \end{aligned} \quad (14)$$

where y_p and y_{p3} represent the vessel-bank distance from the portside to the midship, y_s and y_{s3} are vessel-bank distance from starboard, as shown in Figure 2.

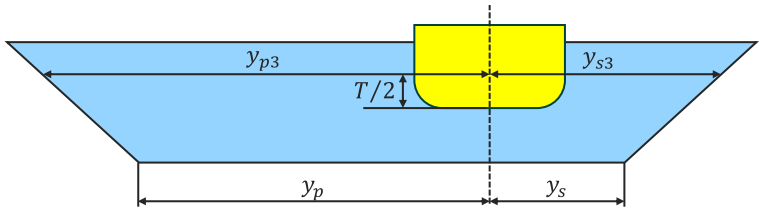

Figure 2. Schematics of vessel-bank distances. The vessel's cross-section is visualised in yellow and is surrounded by the waterway shown in blue.

2.1.6. River current

Current is a critical factor in the inland waterways that might affect vessel dynamics. Specifically in sharp river bends or narrow fairways, the presence of currents makes manoeuvring complex. The currents in this work follow a near parabolic distribution along the lateral direction, meaning that the flow has a higher speed near the waterway's centre and close to zero speed near the banks. The equation is given as:

$$\begin{aligned} u_r &= u - U_C\cos(\beta_C - \psi) \\ v_{rm} &= v_m - U_C\sin(\beta_C - \psi) \end{aligned} \quad (15)$$

where, β_C is the incoming current angle in the earth-fixed coordinate system. Hence, the drift angle at midship, which accounts for the difference between the vessel's course and heading, is given by $\beta_m = -\tan^{-1}(v_{rm}/u_r)$. Further, the total ship speed U is calculated by using $U = \sqrt{{u_r}^2 + {v_{rm}}^2}$. Note that the equations of motion are updated using the vessel's speed through water.

2.2. Guidance, navigation and control for inland waterborne navigation

2.2.1. Navigation system

The guidance and control systems rely on the continuous availability of the vessel's position, heading and velocities in three degrees of freedom (3-DOF). This is made possible by the multiple sensors that typically form a part of the navigation system and facilitate sensor fusion, redundancy and fault diagnosis. Typically, GPS/GNSS, gyrocompass and accelerometers are employed for the same. The navigation system of an IWV can be differentiated from a seagoing vessel by the requirement of additional sensors measuring the water depth and currents that must be incorporated into a closed-loop control system for autonomous navigation. The vessel's distance from the bank must also be available and can be measured using Electronic Chart Display and Information System (ECDIS) data (European Commission, 2020). Additionally, in major rivers and canals, bank infrastructure is increasingly being installed to offer precise localisation with respect to fairway boundaries. Such infrastructure includes fixed beacons and transponders that communicate with the vessel's systems to provide constant updates on its relative position. Advanced navigation systems may further integrate Automatic Identification System (AIS) data and satellite-based augmentation system (SBAS) to improve positioning accuracy and situational awareness.

2.2.2. Guidance system

The IWV path following problem can be posed as a heading control problem by using an appropriate guidance law. This requires transforming the desired position coordinates to the desired heading angles. This is a typical approach followed for vessel control, using steering laws such as Line-Of-Sight (LOS) (Breivik and Fossen, 2008), or its improved variants (Fossen and Lekkas, 2017; Xu et al., 2023). The primary objective of such guidance laws is to adjust the vessel's heading angle to minimise the cross-track error, i.e., the lateral deviation from the desired path. As shown in the next section, focusing on heading control can greatly simplify the control design procedure without trading off the path-following performance.

The guidance system uses a path planning algorithm to compute the reference heading angles for a predetermined path created using a set of waypoints. In this work, a lookahead-based Line-of-Sight (LOS) algorithm is employed (Breivik and Fossen, 2008), as visualised in Figure 3. Firstly, the cross-track error $XTE(t)$ is defined by

$$XTE(t) = \sqrt{\left(x_p(t) - x_{cl}(t)\right)^2 + \left(y_p(t) - y_{cl}(t)\right)^2} \tag{16}$$

where, x_{cl} and y_{cl} are the points at the closest distance from the vessel on the desired path. Similarly, signed XTE ($SXTE(t)$) can be defined as

$$SXTE(t) = \begin{cases} XTE(t), & |\tilde{\pi}| < 0 \\ -XTE(t), & \text{Otherwise} \end{cases} \tag{17}$$

where, $\tilde{\pi}$ is the cross product between the waypoint vector and the ship's position vector, and is equal to

$$\tilde{\pi} = (x_{wp,k+1} - x_{wp,k})(y_p - y_{wp,k}) - (y_{wp,k+1} - y_{wp,k})(x_p - x_{wp,k}) \quad (18)$$

Using the current position of the vessel and the positions of the waypoints, the reference heading is computed as

$$\psi^{ref}(t) = \psi_{wp}(t) - \psi_{cross}(t) \quad (19)$$

where, $\psi_{wp}(t)$ represents the reference heading angle component corresponding to the slope of the line formed by two consecutive waypoints, i.e.

$$\psi_{wp}(t) = atan2(y_{wp,k+1} - y_{wp,k}, x_{wp,k+1} - x_{wp,k}) \quad (20)$$

Further, $\psi_{cross}(t)$ is the reference heading angle component that minimises the cross-track error $XTE(t)$ and is given by:

$$\psi_{cross}(t) = atan2(SXTE(t), X_D) \quad (21)$$

where, X_D is a predefined lookahead distance value corresponding to the reaction distance of the IWV, which depends on the vessel type and its dimensions. In this work, it is selected as a constant positive value.

Since the path is approximated by straight-line segments connected by waypoints, a switching criterion is required to switch between these segments. In this work, the along-track distance-based waypoint switching criterion is employed, where a switch is made when the vessel reaches a predefined distance away from the upcoming waypoint (Breivik and Fossen, 2008).

Remark: Path segment/waypoint switching using a constant distance or circle radius can lead to some sharp changes in the reference heading, resulting in rudder angle oscillations (Naeem et al., 2003). These oscillations can be reduced by a careful selection of the lookahead and the along-track distances. Furthermore, a smoother LOS steering law or switching criteria can significantly decrease this effect (Bakaric et al., 2004; Fossen et al., 2003; Saravanakumar and Asokan, 2011).

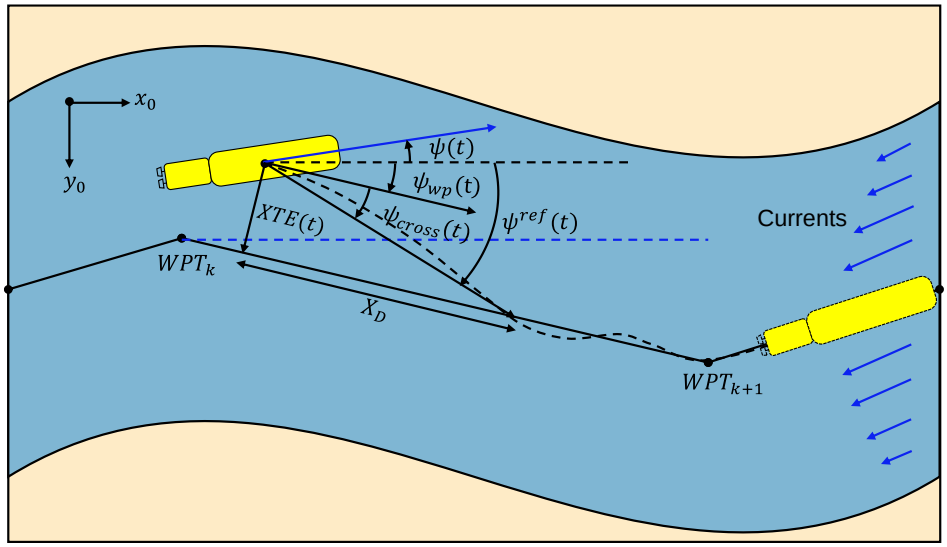

Figure 3. Guidance law for the IWV heading control.

2.2.3. *PID control design*

Figure 4 shows a block diagram representation of the resulting closed-loop system with a PID controller for the IWV heading control. The PID reference tracking control law was designed to update δ_c at each time step, such that:

$$\delta_c(t) = K_p\left(\psi_e(t) + T_d\big(\psi_e(t) - \psi_e(t-1)\big) + \frac{1}{T_i}\left(\sum_{l=0}^{t}\psi_{e_l}\right)\right) \tag{22}$$

where, $\psi_e(t)$ represents the error in the heading angle at the time step t, K_p is the controller's proportional gain and T_d and T_i are the derivative and integral time constants, respectively. To select an optimal value for these control gains, the Ziegler-Nichols method (Ziegler and Nichols, 1942) was employed to ensure a minimal heading error and acceptable overshooting and settling times for the resulting path.

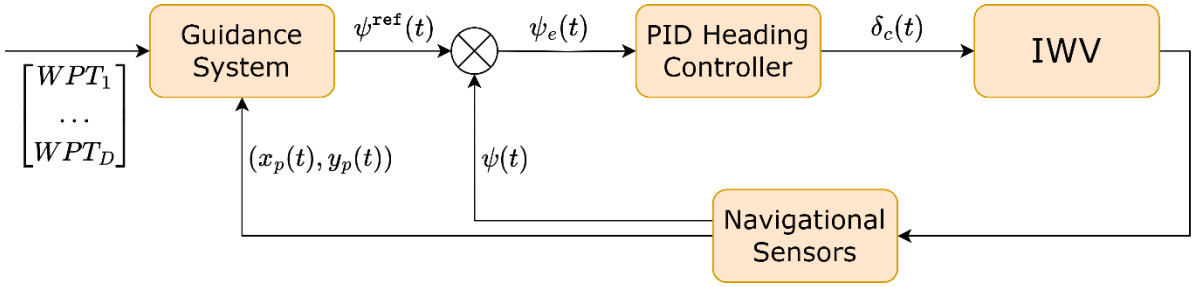

Figure 4. Block diagram representation of the IWV heading control using the PID controller.

2.2.4. *Nonlinear Model-Predictive Control (NMPC): IWV model*

To formulate the NMPC design problem, the IWV dynamics are presented in the state-space notation as:

$$\dot{q}(t) = f\big(q(t)\big) + g_1\big(q(t), \mathfrak{u}(t)\big) + g_2(q(t)) \tag{23}$$

where, $q(t)$ denotes the vessel's states and $\mathfrak{u}(t)$ is the control input, given by:

$$\begin{aligned} q(t) &= [q_1(t) \quad q_2(t) \quad q_3(t) \quad q_4(t) \quad q_5(t) \quad q_6(t)]^T \\ &= [x_p(t) \quad y_p(t) \quad \psi(t) \quad u(t) \quad v_m(t) \quad r(t)]^T \\ \mathfrak{u}(t) &= \delta(t) \end{aligned} \tag{24}$$

Further, the function of vessel states $f\big(q(t)\big)$, $g_2(q(t))$, and of the states and control input $g_1\big(q(t), u(t)\big)$ are given by:

$$\begin{aligned} f\big(q(t)\big) &= \begin{bmatrix} R\big(q_3(t)\big)v(t) \\ -M^{-1}(D - \tau_e) \end{bmatrix} \\ g_1\big(q(t), \mathfrak{u}(t)\big) &= \begin{bmatrix} \mathbf{0} \\ M^{-1}\tau_c \end{bmatrix} \\ g_2(q(t)) &= \begin{bmatrix} \mathbf{0} \\ M^{-1}\tau_o \end{bmatrix} \end{aligned} \tag{25}$$

where:

$$M = \begin{bmatrix} (m+m_x) & 0 & 0 \\ 0 & (m+m_x) & x_G m \\ 0 & x_G m & (I_z + x_G^2 m + J_z) \end{bmatrix}, D = \begin{bmatrix} -\big(m+m_y\big)q_5(t)q_6(t) - x_G m q_6(t)^2 \\ -(m+m_x)q_4(t)q_6(t) \\ x_G m q_4(t) q_6(t) \end{bmatrix},$$

$$\tau_e = \begin{bmatrix} X_H + X_B \\ Y_H + Y_B \\ N_H + N_B \end{bmatrix}, \tau_c = \begin{bmatrix} X_R \\ Y_R \\ N_R \end{bmatrix}, \tau_o = \begin{bmatrix} X_P \\ 0 \\ 0 \end{bmatrix}, R\big(q_3(t)\big) = \begin{bmatrix} cos\big(q_3(t)\big) & -sin\big(q_3(t)\big) & 0 \\ sin\big(q_3(t)\big) & cos\big(q_3(t)\big) & 0 \\ 0 & 0 & 1 \end{bmatrix},$$

and η and ν represent the generalised position and generalised velocity vectors, given by:

$$\begin{aligned} \eta(t) &= [q_1(t) \quad q_2(t) \quad q_3(t)]^T \\ &= [x_p(t) \quad y_p(t) \quad \psi(t)]^T \\ \nu(t) &= [q_4(t) \quad q_5(t) \quad q_6(t)]^T \\ &= [u(t) \quad v_m(t) \quad r(t)]^T \end{aligned} \tag{26}$$

As shown, τ_e comprises the hull forces and bank effect forces, whereas τ_c comprises the controlled rudder forces. Further, note that to simplify the control design process, the propeller rotation speed n_P is uncontrolled and assumed to remain constant during the heading control phase. This assumption is commonly used for path following in inland waterways, as overtaking is rare due to narrow channels, thereby minimising the speed variations. Instead, speed is often optimised as part of the voyage optimization, see for example (Yan et al., 2018).

Equation (23) must be further discretised for a given sampling time to incorporate it as a prediction model within the finite time horizon of the NMPC OCP formulation. Therefore, upon discretisation, the IWV model is derived by the following discrete-time dynamics:

$$q_c(k+1) = f_c\big(q_c(k)\big) + g_{1c}\big(q_c(k), u_c(k)\big) + g_{2c}(q_c(k)) \tag{27}$$

where the subscript $(.)_c$ is used to represent the variables used in the IWV prediction model, and k is the discrete time step. Notice that Equation (27) is highly nonlinear and non-affine in control. Next, the constraints on the state variables and the control inputs are presented through the following inequalities:

$$\begin{aligned} \psi_{min} \leq q_{3_c}(k) \leq \psi_{max} \\ u_{min} \leq q_{4_c}(k) \leq u_{max} \\ v_{min} \leq q_{5_c}(k) \leq v_{max} \\ r_{min} \leq q_{6_c}(k) \leq r_{max} \\ \delta_{min} \leq u_c(k) \leq \delta_{max} \end{aligned} \tag{28}$$

Furthermore, to avoid rudder damage due to excessive actuation, the rate of change of the rudder angle can be limited by enforcing the following inequality:

$$|u_c(k+1) - u_c(k)| \leq \Delta_{max} \tag{29}$$

where, $\Delta_{\max}$ is the maximum allowed change in the rudder angle in one time step. Finally, the fairway constraints can also be better modelled by using polyhedrons in terms of the constraints on the $x-$ and $y-$ coordinates of the vessel, which results in the following inequality constraint:

$$A_{fw}\big[q_{1_c}(k) \quad q_{2_c}(k)\big]^T \leq b_{fw} \tag{30}$$

where, $A_{fw} \in \mathbb{R}^{N_{fw} \times 2}$ and $b_{fw} \in \mathbb{R}^{N_{fw}}$ represent the polyhedron in the H-representation.

2.2.5. NMPC optimal control problem (OCP) formulation

An MPC-based control system computes a finite sequence of optimal control actions online by solving a finite horizon optimisation problem. Out of the computed sequence, only the first control action is provided to the system, and this process is repeated at each time step. Figure 5 represents the overall closed-loop system resulting from the implementation of the NMPC system.

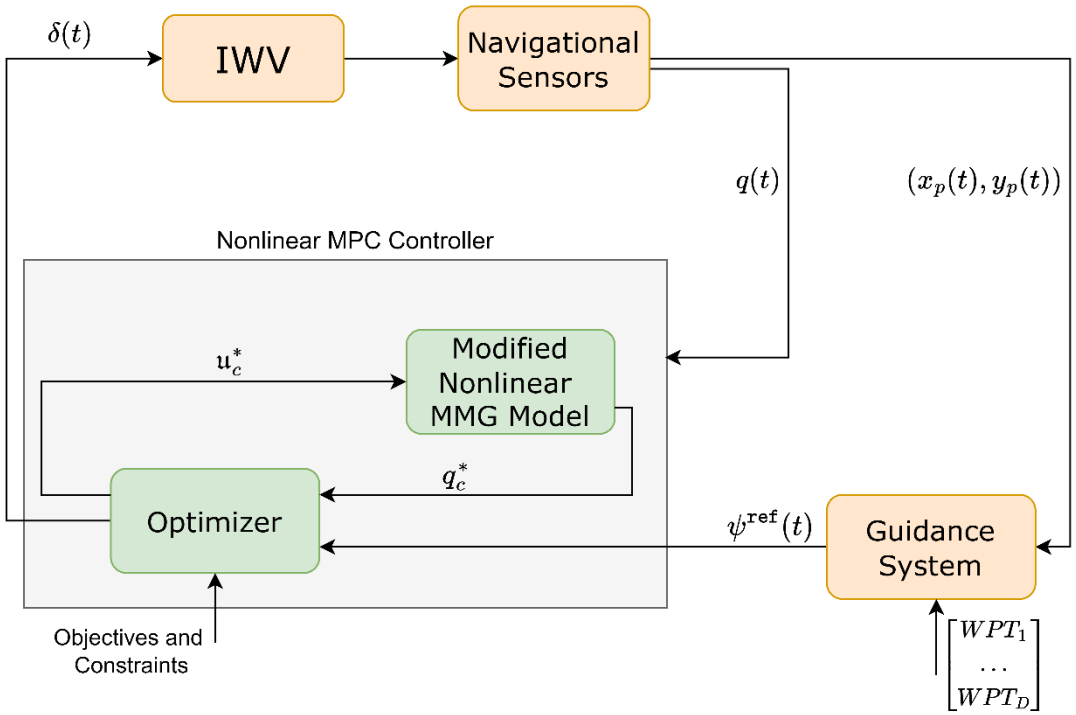

Figure 5. Block diagram representation of the IWV heading control using NMPC.

The NMPC OCP is formulated as a nonlinear programming (NLP) problem using the multiple shooting method over a finite prediction horizon N_h, where at each time step k, the following optimisation problem is solved:

$$NMPC\left(q_{3c}(k), \psi^{ref}(k)\right)$$

$$\begin{aligned} & \underset{q_{3c}, \mathfrak{u}_c}{arg\,min} \left(q_{3c}(N_h|k) - \psi^{ref}(N_h|k)\right)^2 p_m + \sum_{h=0}^{N_h-1} \frac{1}{2}\left(q_{3c}(h|k) - \psi^{ref}(h|k)\right)^2 q_m \\ = \quad & + \mathfrak{u}_c{}^2(h|k) r_m \\ & s.t. \forall h \in 0, \dots, N_h - 1 \\ & q_c(0|k) = q(k), \\ & Eq.(25) - (28) \end{aligned} \tag{31}$$

Here, p_m, q_m, and r_m are scalar values representing the controller weights. Further, h represents a time step over the prediction horizon, such that, $0 \leq h \leq N_h - 1$. Therefore, $h|k$ represents the prediction of the respective variable at the prediction step h, performed at the time step k. The objective function comprises a running cost and a terminal cost component that minimises the heading error. In addition, a running-cost component also minimises the required rudder movements. The solution of the NMPC OCP at the k^{th} time step is the pair of optimal rudder angle sequence and the corresponding sequence of the vessel's states, given by:

$$(u_c^*, q_{3c}^*) = NMPC\left(q_{3c}(k), \psi^{ref}(k)\right) \tag{32}$$

Finally, the first input rudder angle in the sequence is applied to the vessel, such that:

$$\delta(k) = \mathfrak{u}_c^*(0) \tag{33}$$

A unique feature of the multiple shooting method is that it divides the time horizon into smaller segments and generates the state trajectory at each time interval, by solving an independent initial value problem. This is unlike the single shooting method, which propagates the state trajectory from a single initial condition over the entire prediction horizon. This in turn improves the convergence speed of the solution, and makes the optimization more robust to errors in the initial values (Abdelaal et al., 2018).

3. Key Performance Metrics

The IWV heading control involves the satisfaction of multiple objectives. Typically, the controller's performance is evaluated by using the cross-track error and rudder angle error measures. (Du et al., 2022b). In this section, we propose some key performance metrics specifically focussing on evaluating the performance of path-following controllers for IWVs. While some of these metrics are based on commonly used metrics for control analysis, others are focused on evaluating the safety and robustness of inland navigation.

- Maximum Absolute Cross-Track Error (MAXTE): The minimisation of cross-track error (XTE) is the primary objective of IWV heading control. The satisfaction of this objective can be evaluated by using the MAXTE metric, which is given by:

$$MAXTE = \max_k XTE(k) = \max_k \sqrt{\left(x_p(k) - x_{cl}(k)\right)^2 + \left(y_p(k) - y_{cl}(k)\right)^2} \tag{34}$$

  Note that (x_{cl}, y_{cl}) maybe different from the waypoints and correspond to the closest point at a straight-line distance from the vessel. For a pusher connected to multiple barges, it is important to take into account the cumulative width when calculating the MAXTE, and the coordinates (x_p, y_p) must be modified accordingly.

- Average Absolute Cross-Track Error (AAXTE): While MAXTE indicates the maximum deviation from the desired path, AAXTE is concerned with the mean XTE accumulated over the time horizon until the vessel reaches its destination. This metric is also directly related to the running state cost of the NMPC OCP formulation.

$$AAXTE = \frac{1}{T_f} \sum_{k=0}^{T_f - 1} \sqrt{\left(x_p(k) - x_{cl}(k)\right)^2 + \left(y_p(k) - y_{cl}(k)\right)^2} \tag{35}$$

- Safe inland navigation metric (SINM): Assuming two-way traffic on the waterway, it is desired to ensure that the vessel does not deviate too far in the port side direction. For a constant width of the river channel, this corresponds to the vessel not crossing the waterway axis. At the same time, it must have a minimal *XTE*. These constraints can be simultaneously evaluated by using the SINM metric given as

$$SINM = \frac{1}{T_f} \sum_{k=0}^{T_f - 1} \left(\alpha \frac{max(0, XTE(k) - XTE_{max})}{XTE_{max}} + \beta \frac{max\left(0, d_{cl,min} - d_{cl}(k)\right)}{d_{cl,min}} \right) \tag{36}$$

where, $XTE(k)$ is the cross-track error at the time step k, $XTE_{\max}$ is the maximum allowable cross-track error, d_{cl}(k) is the distance of the vessel from the centreline at the k^{th} time step, and $d_{cl,\min}$ is the minimum allowable distance from the centreline. The terms α and β are scalars used to assign weights to the importance of XTE and d_{cl}.

- Average Absolute Control Effort (AACE): The AACE metric computes the average control effort expanded by the control system throughout the duration of the course. It is a crucial metric from the energy consumption point of view. Similar to AAXTE, AACE considers the time-varying profile of the commanded rudder angles δ. This metric is expressed as:

$$AACE = \frac{1}{T_f}\sum_{k=0}^{T_f-1}|\delta(k)|^2 \tag{37}$$

- Inland Waterway Robustness Index (IWRI): As river currents, shallow-water effect and bank effect are some of the most significant sources of external disturbances impacting the IWV manoeuvring, it is crucial to ensure that the designed controller is sufficiently robust against them. The IWRI is calculated by measuring the impact of these disturbances on performance metrics such as the cross-track error and the heading error, by comparing it to a nominal baseline scenario. It is calculated as:

$$IWRI = \frac{1}{T_f}\sum_{k=0}^{T_f-1}\left(\frac{XTE_k - XTE_{bl}}{XTE_{bl}} + \frac{\psi_{e,k} - \psi_{ebl}}{\psi_{ebl}}\right) \tag{38}$$

where XTE_k and $\psi_{e,k}$ are the cross-track errors and the heading errors at the k^{th} time-step, whereas XTE_{bl} and ψ_{ebl} are the corresponding baseline errors under nominal conditions. The baseline errors can be calculated by estimating the achievable errors under no water current, shallow-water and bank effect conditions.

- Estimated Time of Arrival (ETA): The vessel's ETA can vary significantly despite it maintaining a constant propeller rpm due to environmental factors such as currents, wind, and hydrodynamic disturbances. The controller's ability to effectively predict and counteract these factors plays a crucial role in determining the actual sailing time. For simplicity, the ETA is calculated while assuming no traffic congestion and the vessel being able to maintain a constant propeller speed throughout its journey.

$$ETA = \frac{D}{v} + \sum_{i=1}^{n}\left(\frac{\Delta d_i}{v - \Delta v_i}\right) \tag{39}$$

Here, n distance segments are considered where speed deviations are caused due to various factors. D and v denote the total distance to be covered and the constant nominal speed of the vessel, whereas Δd_i, Δv_i denote the $i-$th distance segment with speed variation, and the variation in speed, respectively.

Ideally, it is preferred that these performance metrics have the minimum possible values. For SINM, the ideal value is zero, whereas for IWRI, a negative value indicates the controller outperforming the nominal case. In the following subsections, various simulation scenarios are presented to further evaluate the proposed controller's performance against these metrics.

4. Simulation Results

This section shows the simulations of pusher-barge trajectories with designed controllers. The modified MMG model is utilised as the basis for predicting vessels' dynamics under inland waterways with current effects. The simulation scenarios cover three typical operational modes of IWVs: (i) navigation along one side of the bank in the straight canal, (ii) turning in waterway interactions confluence, and (iii) track-pilot along river bends. The performance and robustness of the proposed control methods are evaluated by the deviation of course (cross-track error) and rudder efforts, as well as the proposed key performance metrics.

4.1. Vessel model

The vessel considered in this work is a pusher-barge convoy, where a rake barge connects to a pusher to formulate the 11BP system, as shown in Figure 6. The geometry of the convoy is listed in Table 1. Note that the midship position for the vessel is defined at the longitudinal and latitudinal coordinate representing the centre of the entire convoy, i.e., $(50.48, 0)$ m. The pusher has twin ducted propellers and four rudders to generate adequate manoeuvrability. The profile of the propeller and rudder is shown in Table 2. The hydrodynamic derivatives are selected based on experimental data from Koh and Yasukawa (2012), the model test was conducted on various water depth conditions, including depth-to-draught ratio (H/T) of 1.5 for medium shallow water and 1.2 for shallow water conditions (see the Table 3).

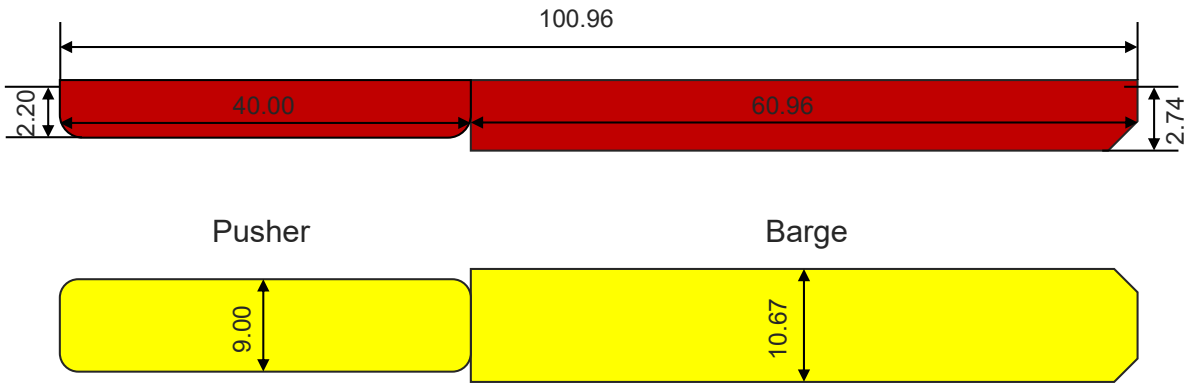

Figure 6. Geometry of pusher-barge convoy; dimensions in meters.

Table 1. Dimensions of the pusher-barge convoy in full-scale.

Parameters	Pusher	Rake-barge	Pusher-barge convoy
Length, L [m]	40.00	60.96	100.96
Ship Beam, B [m]	9.00	10.67	10.67
Draught, T [m]	2.20	2.74	2.74
Displacement, ∇[m^3]	494.7	1646.2	2140.9
Block coefficient, C_B [-]	0.633	0.924	0.725

Table 2. Profile of rudder and propeller equipped on the pusher.

Parameters	Values
Propeller diameter, D_P [m]	1.8
Revolution speed, n_P [rpm]	300
Rudder span, B_R [m]	2.0
Rudder chord length, C_R [m]	2.0

Rudder area, A_R [m^2]	4.0

Table 3. Hydrodynamic derivatives of the pusher-barge model in shallow water.

Symbol	H/T=1.5	H/T=1.2	Symbol	H/T=1.5	H/T=1.2
$X'_{\beta\beta}$	−0.1749	−0.3637	m'_x	0.0148	0.0195
X'_{rr}	0.0792	0.1055	m'_y	0.2325	0.3722
$X'_{\beta r}$	−0.0888	−0.248	t	0.249	0.326
Y'_{β}	0.6354	1.2375	α_H	0.089	0.418
Y'_{r}	−0.0227	−0.113	x'_H	−0.249	−0.189
$Y'_{\beta\beta\beta}$	2.5353	4.2245	w_{PO}	0.493	0.576
$Y'_{\beta\beta r}$	0.7413	3.6005	γ_R	0.357	0.293
$Y'_{\beta rr}$	0.286	0.7129	ℓ'_R	−0.538	−1.113
Y'_{rrr}	−0.0836	−0.2003	ε	1.189	1.823
N'_{β}	0.1988	0.4435			
N'_{r}	−0.0654	−0.0861			
$N'_{\beta\beta\beta}$	0.5665	1.1277			
$N'_{\beta\beta r}$	−0.6547	−0.2249			
$N'_{\beta rr}$	−0.0528	−0.0561			
N'_{rrr}	0.0097	−0.0522			

4.2. Control parameters

The simulation scenarios are implemented based on the controller parameters listed in Table 4. For the NMPC, the state constraints are derived from the practical physical limits of the IWV. A prediction horizon equal to 25 secs is selected based on the full-scale vessel's characteristic time-scale and a computational requirement that enables for real-time application. Furthermore, the OCP is formulated using the Casadi toolbox (Andersson et al., 2019) and solved using IPOPT (Wachter and Biegler, 2006). The NLP formulation of the OCP is performed using the multiple-shooting method in MATLAB to ensure improved efficiency and numerical stability.

Table 4. Parameters of the controllers.

Controller	Parameter	Value
PID	K_P	5
	T_I	10
	T_D	25
	Time interval [sec]	0.5
NMPC	Prediction horizon N_h[sec]	25
	Interval [sec]	0.5
	Terminal cost weight p_m	4500
	Running cost weights q_m, r_m	$q_m = 150, r_m = 1 \times 10^{-4}$
	Rudder angle limits [degrees]	$-45 \leq u_c(k) \leq 45$
	Heading angle limits [degrees]	$-90 \leq q_{3c}(k) \leq 90$
	Surge velocity limits [m/s]	$0 \leq q_{4c}(k) \leq 5$
	Sway velocity limits [m/s]	$-1.5 \leq q_{5c}(k) \leq 1.5$
	Yaw velocity limits [degrees/s]	$-5 \leq q_{6c}(k) \leq 5$
	Rudder angle change rate Δ_{max} [degrees/sec]	7.2

4.3. Straight channel simulation

The straight channel is designed to have a width of W_C=100 m, and a rectangular cross-section with a constant water depth of H/T=1.2, representing extreme shallow water conditions that might pose challenges to steering handling. The currents are near parabolic and distributed along the canal with the maximum current speed at the waterway centre (U_{CMAX} = 0.5 m/s). The vessel is desired to keep a constant lateral vessel-bank distance of y_s= 25, which is a typical operational condition to ensure safety in confined canals to clear the way for upcoming or overtaking vessels. Under this circumstance, the heading controller is responsible for compensating the disturbances due to complex hydrodynamic effects from waterway, such as shallow water effect, bank effect and currents, to track and maintain the desired course with minimum error and control effort.

Figure 7 showcases the vessel trajectory with PID controller and NMPC under the influence of water currents. For upstream sailing, it can be observed in Figure 7 (a) that both controllers show good performance as the trajectories are fairly close to the reference path. Under downstream conditions in Figure 7 (b), the heading controller can maintain the path effectively while a slight course deviation can be noticed. This is due to the decrease of rudder incoming flow speed at downstream navigation for lower steering force. This phenomenon can be clearly seen in Figure 8, where the rudder effort is obviously lower in the upcoming current (Figure 8 (a)) as compared to downstream sailing, as shown in Figure 8 (b). The comparison of rudder effort also emphasises an important feature of NMPC: optimisation of the control effort. The controller can effectively utilise its predictions over the future horizon to adjust the rudder instead of correcting only based on the vessel's states, as in the case of PID control. The cross-track error is shown in Figure 8 (c) and (d), and in general, the time plot shows both controllers have good tracking performance, with the NMPC having an even smaller cross-track error. Especially in upstream conditions, the lateral course deviation converges to less than 0.5 m from the desired track. When navigating in narrow fairways, such as locks or small canals, precise motion control and track-keeping are critical for ensuring navigational safety.

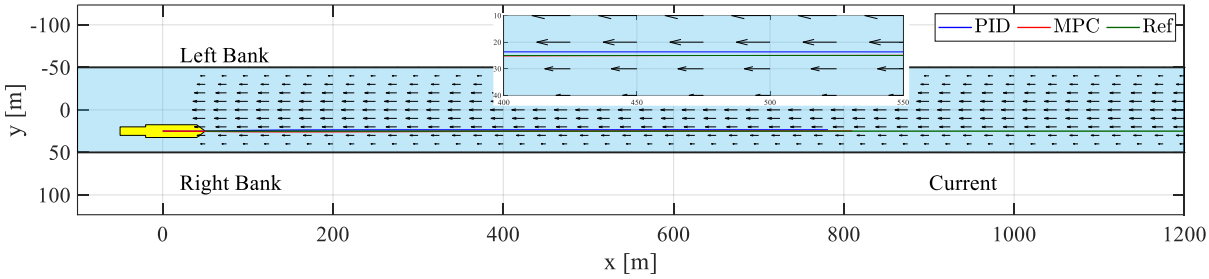

(a) Trajectory of upstream sailing.

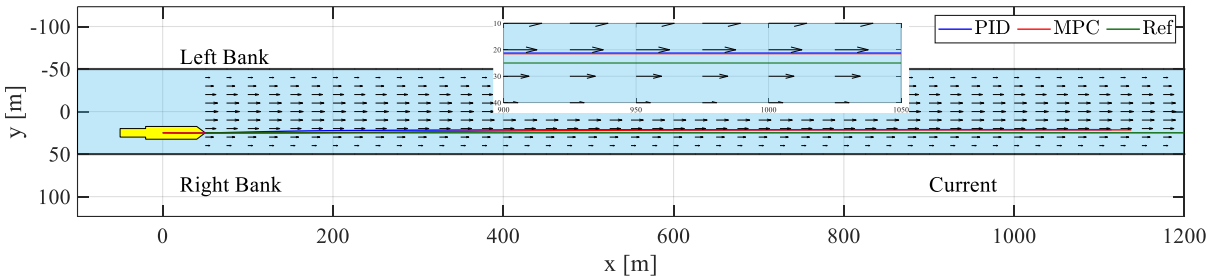

(b) Trajectory of downstream sailing.

Figure 7. Trajectories in a straight channel under heading control.

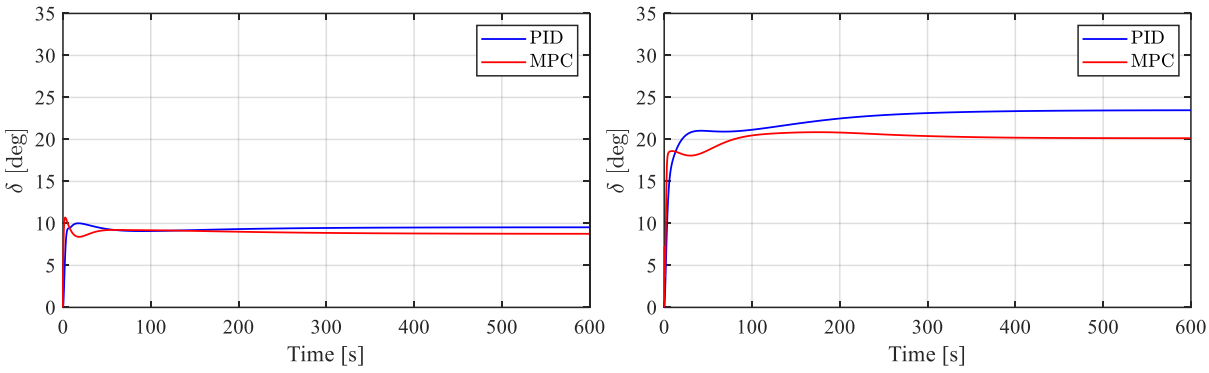

(a) Rudder angle (upstream).

(b) Rudder angle (downstream).

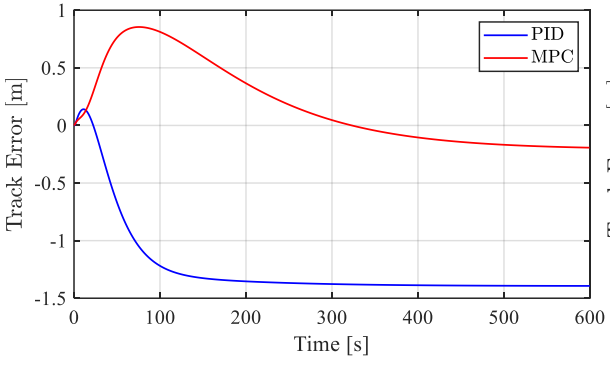

(c) SXTE (upstream).

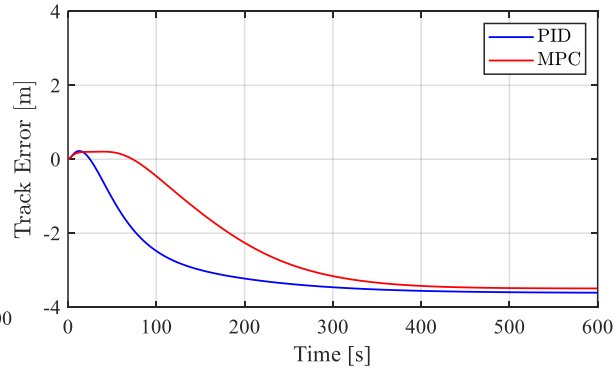

(d) SXTE (downstream).

Figure 8. The rudder angles and signed cross-track errors (SXTE) (see Equation (20)) over time with PID controller and NMPC for the vessel sailing upstream and downstream, respectively.

4.4. T-junction simulation

Inland waterways have many intersections that connect river branches, canals, and ports to form complex transport networks. Navigating a vessel through this waterway confluence faces unique challenges, such as tight manoeuvres or sharp turning. Unlike sea-going vessels, the operational spaces

of IWVs are limited by such waterways. Therefore, advanced heading control is critically important when steering vessels in these intersections. To evaluate the tracking performance of the designed controllers, a waterway intersection with a "T-junction" shape is established in this section. The main channel has a relatively higher current speed (U_{CMAX}=0.5 m/s), and the tributary has a lower current speed (U_{CMAX}=0.1 m/s). It should be noted that the hydrodynamic behaviour of flow at the confluence point, such as vortices, is neglected in this work as it requires CFD simulation with accurate turbulence models. To execute a sharp turn in confined water, the vessel must initiate the manoeuvre well in advance. This implies that the waypoint generation should take the vessel's turning behaviour into consideration. In this scenario, the starting point for turning was selected based on the vessel's advance distance, which is equal to 2.5 times the vessel's length (Zhang et al., 2024b).

Figure 9 illustrates the trajectories resulting from the turning simulation under different current directions in the main channel, where attitudes of the vessel have been plotted in different colours to show its turning dynamics along the corresponding trajectory. To ensure turning safety, the vessel maintains a relatively low constant propulsion speed of 100 rpm, meaning that the speed changes dynamically only according to the vessel's location and current directions, as shown in Figure 10. The trajectories indicate that the NMPC achieves a near-perfect tracking performance under both conditions. In the downstream current as depicted in Figure 9 (a), the difference between the PID controller and NMPC is relatively minor, as the incoming current increases the rudder load and generates more manoeuvring force, although some course deviation from the PID controller is still observable. In contrast, when applied to the downstream current scenario (see Figure 9 (b)), a clear difference between the two control methods can be seen. The PID controller exhibits a significantly higher tracking error compared to the NMPC, with the maximum tracking error even exceeding 20 m during the turning simulation, as shown in Figure 11. Another important factor that should be noted is that while the tracking performance of the PID controller is inferior to the more advanced NMPC, it still enables the system to generate fast responses to dynamic environmental impacts. As shown in Figure 9 (b), when the vessel completes the turn and enters the tributary, the PID controller's heading control can quickly steer the vessel back to the desired track, highlighting the controller's ability to adapt swiftly to changing conditions.

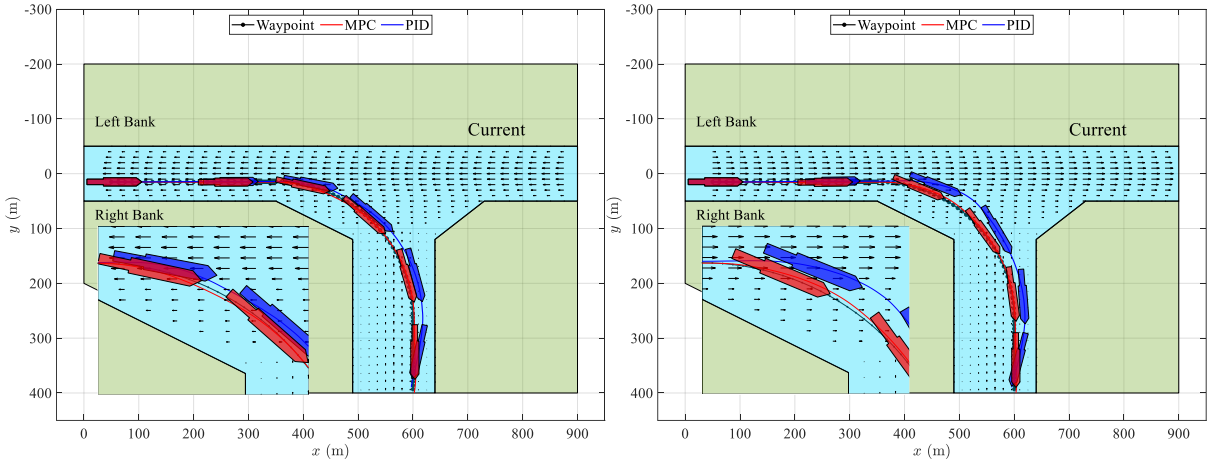

(a) Trajectory under upstream current. (b) Trajectory under downstream current.

Figure 9. Comparison of trajectories in T-junction-shaped waterways with a consistent water depth condition of H/T=1.2. The vessel keeps a constant propulsion speed of 100 rpm.

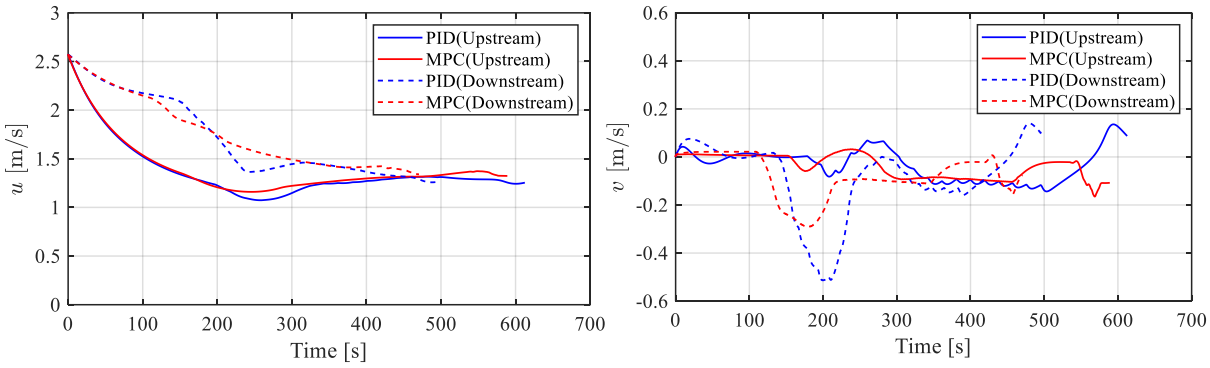

(a) Surge speed u. (b) Sway speed v.

Figure 10. Comparison of the surge velocity u, v during vessel turning, for PID controller and NMPC.

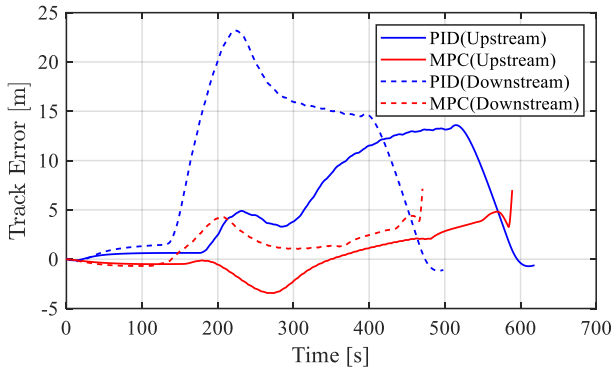

Figure 11. The signed cross-track errors with PID controller and NMPC for the vessel sailing upstream and downstream, respectively.

The corresponding rudder control effort is summarised in Figure 12. The rudder angle indicates a clear difference between the PID controller and NMPC. The NMPC's objective function explicitly considers reducing control effort, resulting in smoother and more consistent rudder angles over time. As seen in the NMPC simulations, the rudder angle does not show sudden changes during most of the operational period. However, relatively large deflections are observed in a short period when the vessel enters the near-bank track in the tributary due to the need for the heading controller to compensate for newly encountered hydrodynamic disturbances and maintain the vessel's course. On the contrary, the PID heading controller results in large deflections under both current directions. This difference highlights the potential of the NMPC to reduce frequent changes in the steering system, which is crucial for energy conservation and the stability of autonomous systems, especially as future IWVs may be fully electrified.

Additionally, in this work, the vessel follows a constant rpm since vessels typically do not frequently change speed while navigating in a straight line. Implementing speed control within a certain range during sharp turns could potentially enhance the controller's performance in course tracking. However, this approach would also increase the complexity of the control design. Both controllers would require more parameter tuning due to the introduction of additional control variables. Furthermore, the computational demand will be higher when solving the NMPC optimisation problem online, necessitating more advanced hardware to ensure real-time performance.

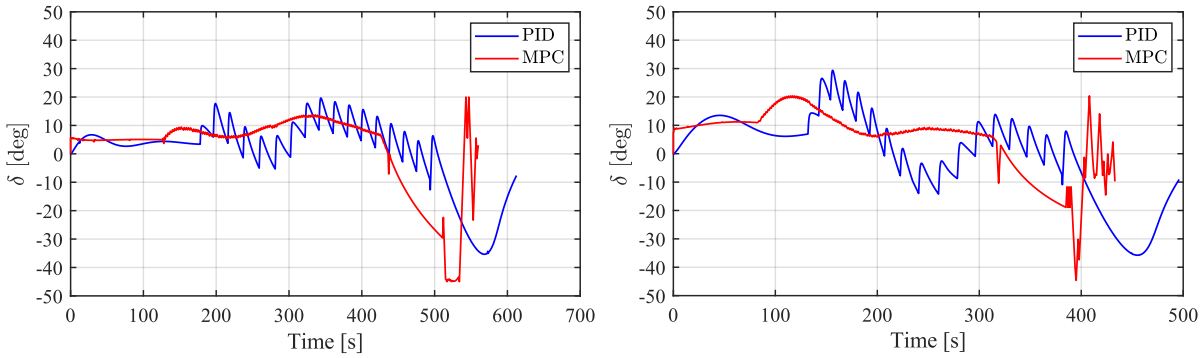

(a) Rudder execution for upstream case. (b) Rudder execution for downstream case.

Figure 12. The rudder angles over time with PID controller and NMPC for the vessel sailing upstream and downstream, respectively.

4.5. River bends simulation

The final simulation scenario is navigation over river bends, which is the most prevalent environment for natural rivers. In this section, a river with near-wave-shaped bends is defined. The channel has a constant width of 150 m and a uniform water depth (H/T=1.2), which corresponds to the shallow water condition described in Section 4.4. The current flow follows the direction of the waterway, reaching its maximum speed in the centreline. Figure 13 depicts the trajectories obtained from the vessel's closed-loop simulations in river bends. The vessel begins at an initial vessel-bank distance (y_s) of 55 m and maintains a constant propulsion speed of 100 rpm. The control objective is to steer the vessel towards a predefined route at a lateral distance of 35 m from the bank. Overall, the results suggest that both control methods provide good tracking performance since the vessel can follow the course effectively. It is noteworthy to note that, in this scenario, the PID controller outperforms the NMPC at the start of the simulation since it can steer the vessel faster to approach the track. This aligned with the findings in the Section 4.4, demonstrating the capability of the PID controller to react quickly. Because current fields grow more complicated near river bends, the NMPC must account for these additional dynamic disturbances within the same prediction time. This can explain its initial struggle at optimisation, especially in the downstream case with reduced rudder capacity (see Figure 13 (b)). Once the interaction increases, the NMPC follows the course while providing a good tracking performance. This can be seen in the time plot of the cross-track error, where the comparison showcases that NMPC can effectively reduce course deviation (see Figure 14). At the second river bend, where x spans from 800 to 1200 m, the XTE from NMPC remained steady at less than 5 m, whereas the PID controller had nearly twice the value. Similarly, the rudder angle oscillations are also significantly larger for the PID controller for both upstream and downstream sailing cases (Figure 15), even reaching its maximum angle limit of 45 degrees.

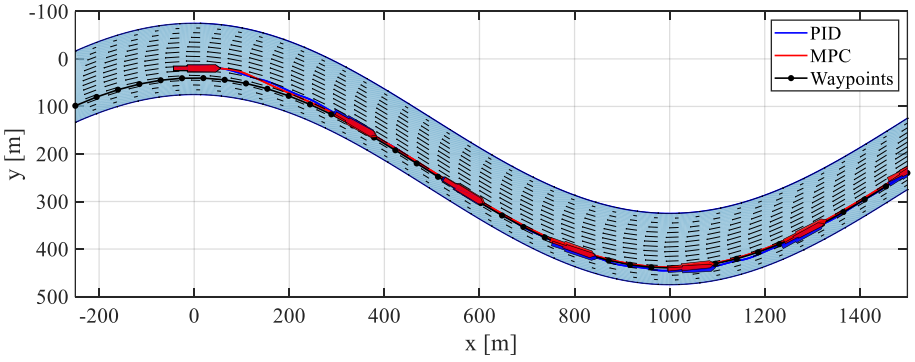

(a) Trajectory of upstream sailing.

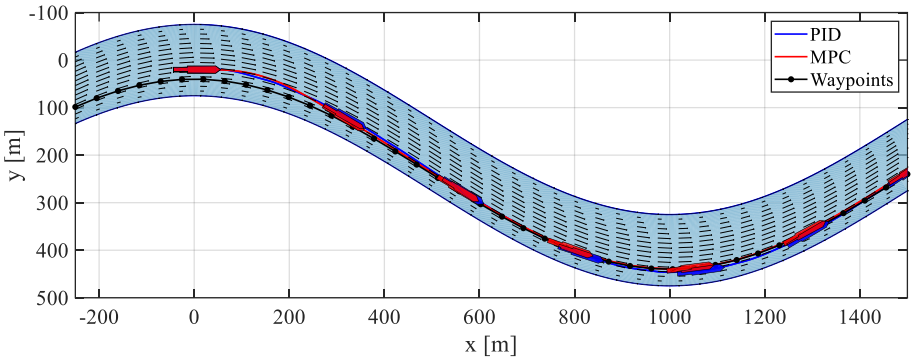

(b) Trajectory of downstream sailing.

Figure 13. Trajectories of control simulations on river bends.

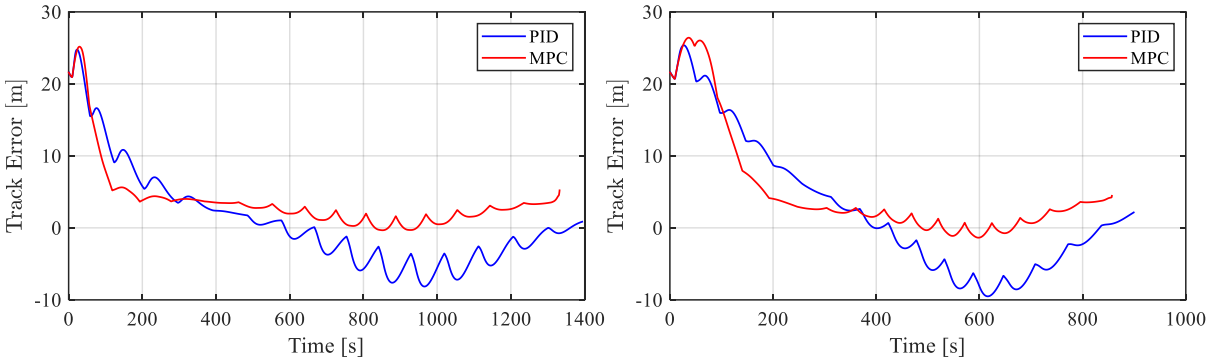

(a) SXTE for upstream sailing case. (b) SXTE for downstream sailing case.

Figure 14. Comparison of signed cross-track errors with PID controller and NMPC for the vessel sailing upstream and downstream, respectively.

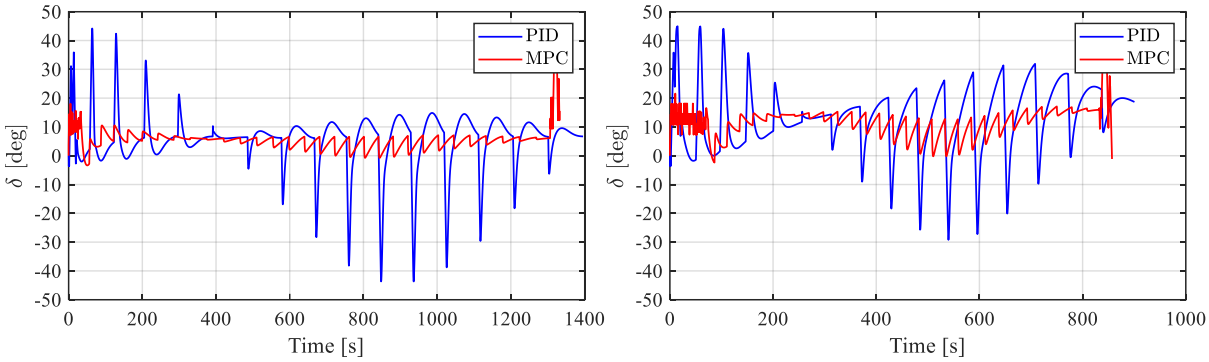

(a) Rudder angles for upstream sailing case. (b) Rudder angles for downstream sailing case.

Figure 15. Rudder angle plots for river bend navigation for the vessel sailing upstream and downstream, respectively.

4.5.1. Impact of ship-bank distances

IWVs frequently need to sail close to riverbanks to facilitate the passage of other vessels. However, vessels may experience significant hydrodynamic effects when navigating very close to the banks. The impact of bank effects is investigated under different ship-bank distances to evaluate the performance of the control design. Figure 16 showcases the trajectories under two ship-bank distance conditions. The vessel is expected to follow the designated path with heading control to maintain its course, under disturbances caused by increasing levels of bank effects. The NMPC can effectively control the heading deviation at a medium ship-bank distance (y_s=30). However, it is important to note that the closer the

vessel is to the bank, the more pronounced the bow-out moment acting on it becomes, see Figure 16 (b). When the route is extremely close to the bank, both controllers face difficulties in steering the vessel back to the desired track. It can be observed from the rudder angle plots (Figure 17) that the PID controller expends higher control effort in the form of large rudder deviations to maintain the reference trajectory, whereas the NMPC makes smaller but more frequent rudder deviations.

Considering the vessel's response time, such scenarios of navigating very close to riverbanks are particularly challenging. Future research should focus on developing more refined control designs, such as reducing speed while ensuring sufficient rudder steering force.

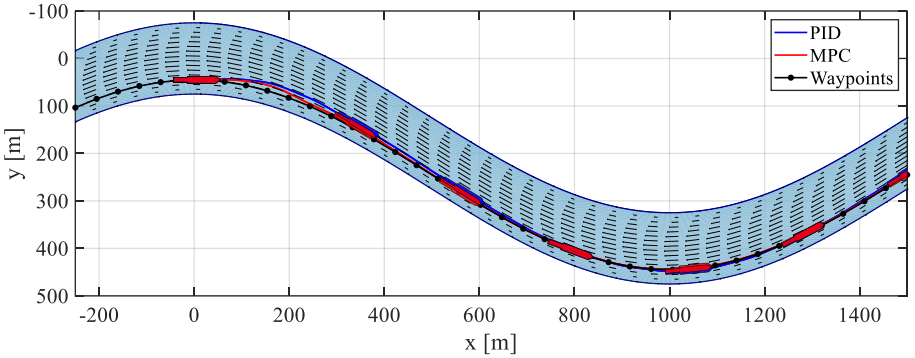

(a) Trajectory under y_s=30.

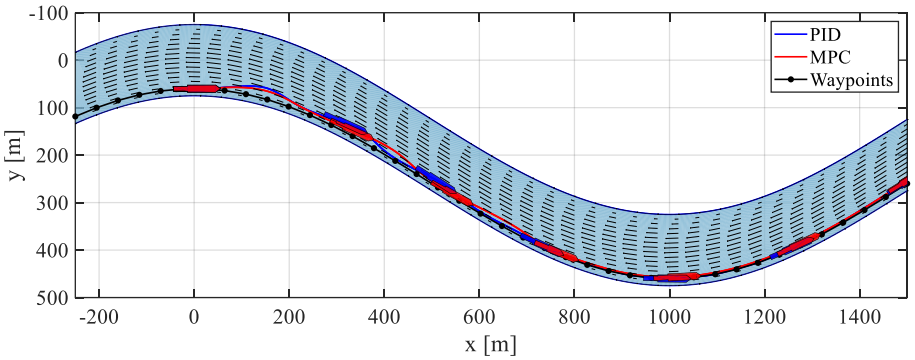

(b) Trajectory under y_s=15.

Figure 16. Trajectories under different ship-bank distances.

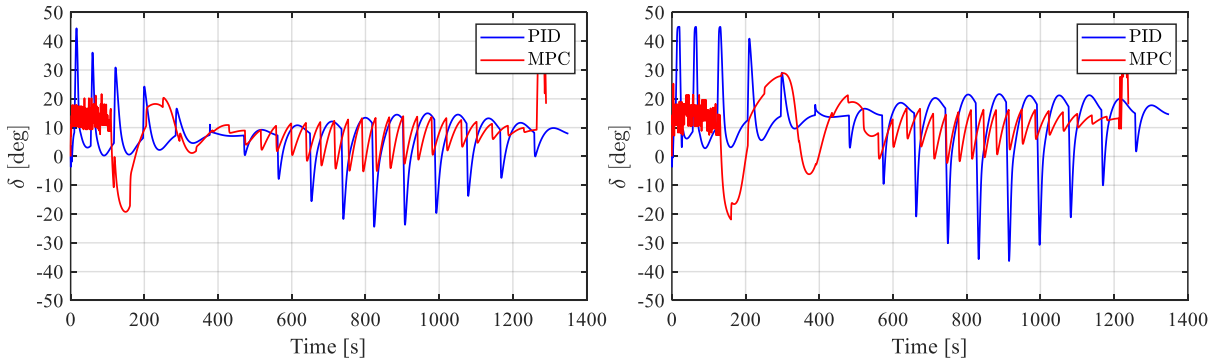

(a) Rudder angle under y_s=30. (b) Rudder angle under y_s=15.

Figure 17. Rudder angle plots under different ship-bank distances.

4.5.2. Impact of propulsion speeds

In this subsection, the impact of shaft speed on control performance is analysed for three different RPMs: 100, 125 and 150. The initial simulation setup was kept consistent with the aforementioned conditions. The cross-track errors of the two algorithms at different speeds are presented in Figure 18. The results indicate that increasing speed can reduce the tracking error by utilising higher rudder force, as shown in Figure 18 (a). However, in the case of the PID controller, increasing speed does not improve the vessel's tracking performance; instead, it introduces higher deviations. This may be attributed to the characteristics of the NMPC, which incorporates a prediction model. This is crucial for allocating the control inputs appropriately based on anticipated vessel behaviour in future steps. In contrast, the increased rudder load does not yield the expected benefits with the PID controller, as the rudder may oversteer due to shorter reaction times at higher speeds. Additionally, it is noteworthy that the NMPC can align the vessel with the reference trajectories with minimal track error, significantly reducing the sailing time while ensuring minor course deviations. For instance, the blue line (100 rpm) indicates that the NMPC saves almost 200 seconds of operation time as compared to the PID controller. This is crucial for reducing the ETA and saving energy, especially during long-term operations.

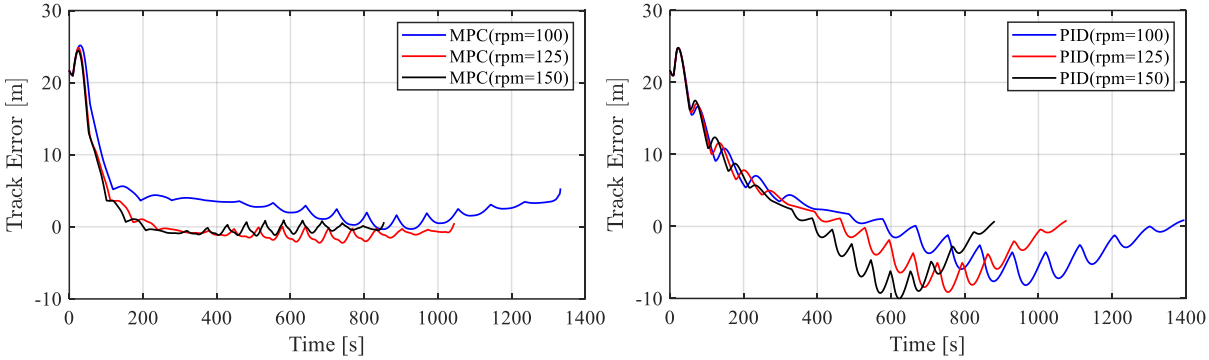

(a) SXTE of NMPC. (b) SXTE of PID.

Figure 18. The impact of propulsion speeds on the signed cross-track error with PID controller and NMPC. The vessel is sailing upstream in these scenarios.

4.5.3. Impact of river cross-section shapes

In previous sections, the channel has a rectangular-shaped cross-section. In natural inland waterways, the fairway has different bank geometry with varying slopes. A common cross-section shape is trapezoidal, with a constant slope from the bottom up to the free surface. In this section, the impact of the cross-section shape is analysed and quantified with three bank slopes. The channel's top width is 150 m, and the bottom width varies from 120 m to 80 m. The maximum water depth is 1.5 times the vessel's draught (H/T=1.5) to represent medium shallow water, and it decreases near both sides of the banks. The cross-sectional shape and waterway generated from the top view are illustrated in Figure 19. The control objective for the vessel is to keep a constant distance of 40 m from the bank ($y_s = 40$). This suggests that the narrower the bottom width, the more confined the waterways are and the stronger the hydrodynamic force (bank-effect) acting on the vessel. Under this scenario, the initial rpm is set to 100 according to the speed's impact on the performance of both controllers in the section 4.5.2.

In the case of a relatively wider bottom, as shown in Figure 20, some deviations between the two controllers have been noticed. The PID controller shows higher course deviations at the beginning, and the error gradually converges with good tracking performance over time (blue line). It is clear that the PID controller shows difficulties in course tracking due to the bank effect. For NMPC simulation, as

illustrated in the blue line, the vessel is also subject to a bow-out effect at the beginning, but proactive heading control effectively mitigates the course deviation, and the trajectory does not show much oscillation behaviour. When the waterway becomes more constrained, the channel wall poses a stronger hydrodynamic force and moment on the vessel, making the tracking performance in the case of the PID controller worse, as obvious deviations can be observed. The NMPC is affected by such stronger bank effects as well, but the trajectory is more stable and still follows the desired track, as shown in Figure 21 and Figure 22. A quantitative analysis of the signed cross-track error and the rudder angles is presented in Figure 23 and Figure 24, respectively, which compares the performance of each controller for the considered cases. The NMPC demonstrates excellent tracking ability with lower rudder efforts under a variety of waterway constraints. The increasing bank effect results in slightly increased tracking error, but the heading control can limit deviations to a very promising range (below 5 m) in all instances. In contrast, the PID controller has a considerable steady cross-track error at the second bend, which is almost twice that of the MPC. Such a value is considered a large course deviation, as the vessel may risk a loss of manoeuvrability when approximating channel banks.

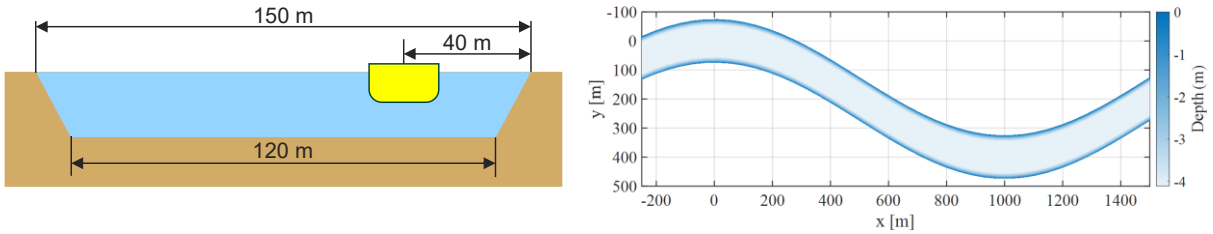

(a) Slope 1: w_{CB}=120.

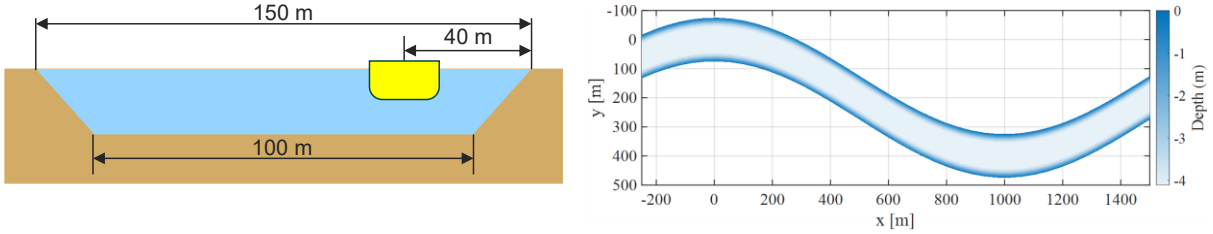

(b) Slope 2: w_{CB}=100.

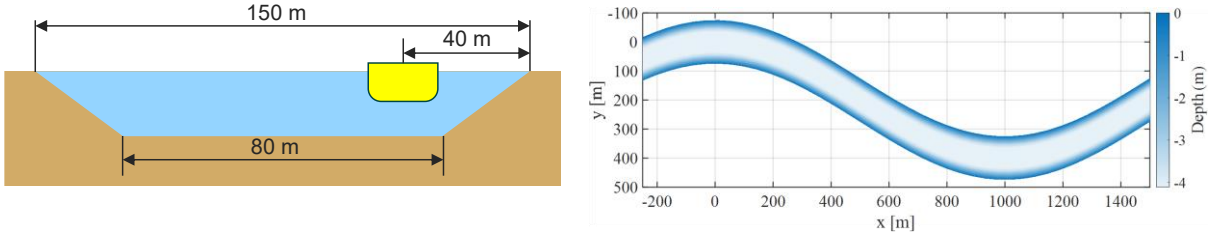

(c) Slope 3: w_{CB}=80.

Figure 19. Waterway generation with different cross-section shapes.

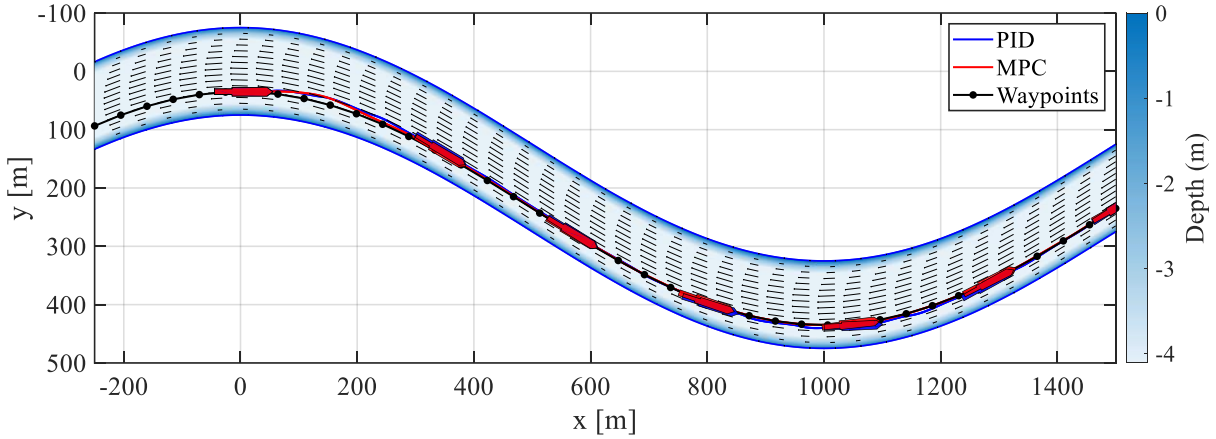

Figure 20. Trajectories in river bends with a bottom width of W_{CB}=120m.

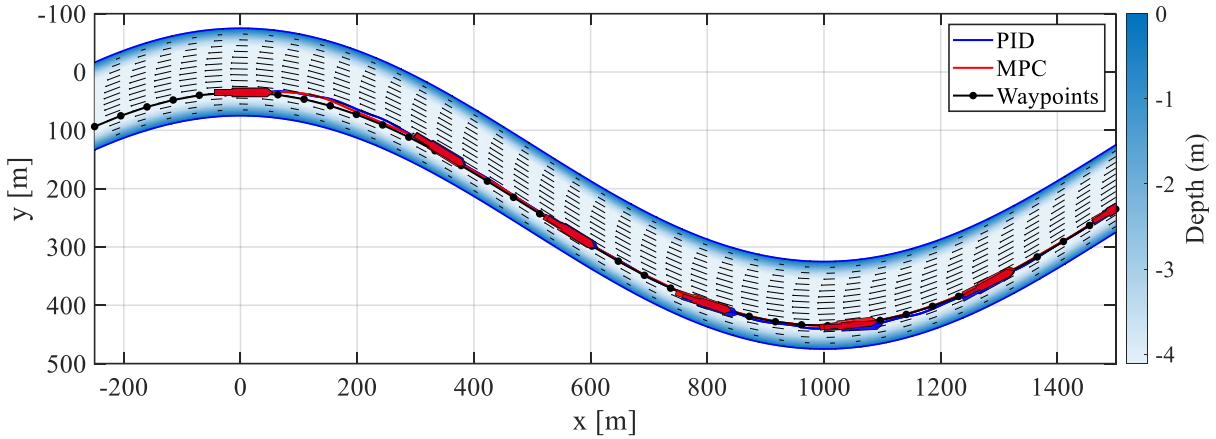

Figure 21. Trajectories in river bends with bottom width of W_{CB}=100m.

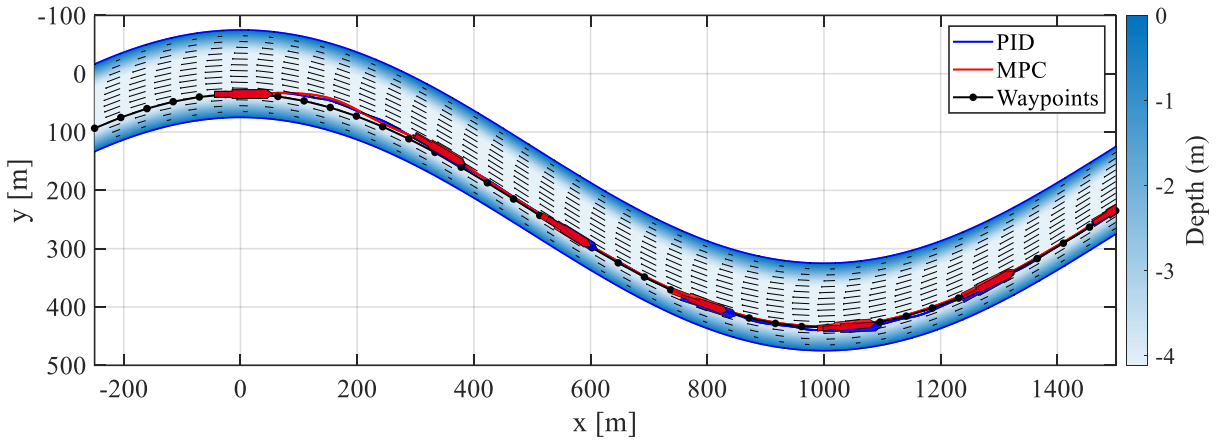

Figure 22. Trajectories in river bends with bottom width of W_{CB}=80m.

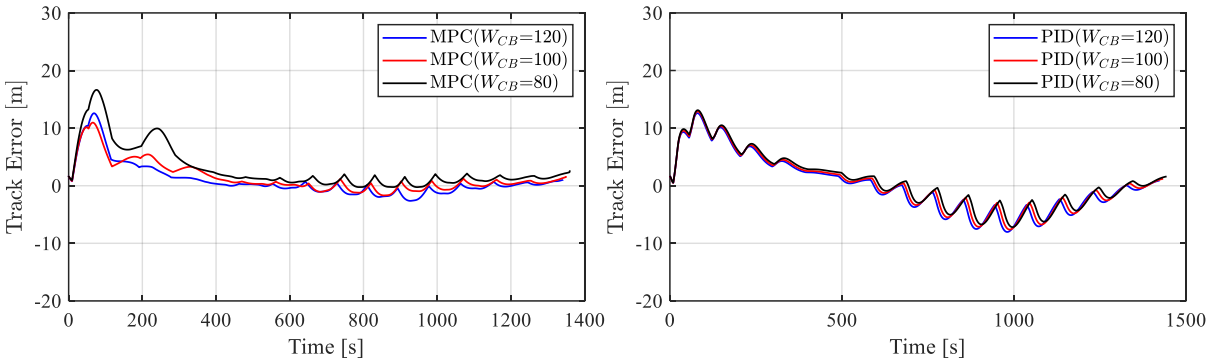

(a) SXTE of NMPC. (b) SXTE of PID.

Figure 23. Signed cross-track error comparison with PID controller and NMPC under varying width of the river bottom.

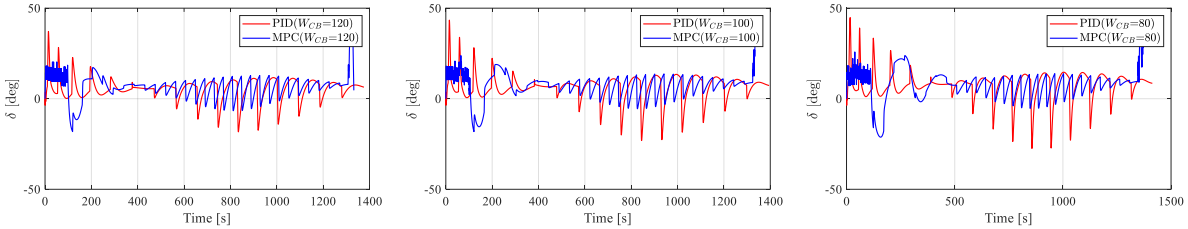

Figure 24. Rudder angles for the PID controller and NMPC under varying width of channel bottom.

4.6. Comparison of key performance metrics

In this subsection, the performance of the proposed NMPC is further analysed and compared with the traditional PID controller by using the key performance metrics proposed in subsection 2.3. For the SINM metric, the parameters α and β are selected to be equal to 0.5. Further, XTE_{max} and $d_{cl,min}$ are selected as 1.7, 10 meters for the straight channel and 2.5, 5 meters for the T-junction and river bends scenario, respectively. For the IWRI metric, the XTE_{bl} and ψ_{ebl} are selected as 0.15 meters, 0.01 radians for the straight channel, and 1.5 meters, 0.07 radians for the T-junction and river bends scenarios, respectively.

As seen in Table 5, the values obtained for NMPC are significantly lower than the ones for the PID controller for most metrics in both upstream and downstream cases. The PID controller outperforms NMPC only in the AACE metric in the straight channel and river bends simulation, and in the MAXTE metric in the river bends case. However, the higher MAXTE value for NMPC is due to a sharper initial heading computed by it for steering the vessel. This ultimately leads to a smaller average XTE, as indicated by the AAXTE metric. Interestingly, the IWRI metric has a negative value in the T-junction scenario for downstream sailing with NMPC, highlighting its robustness as compared to the baseline values. The NMPC also takes significantly less time to reach the destination in all three scenarios, as captured by the ETA metric.

Table 5. The values of the key performance metrics for the considered simulation scenarios. For each scenario, the minimum values obtained are highlighted in bold.

Scenario	**Current stream**	**PID**						**NMPC**					
		MAXTE	AAXTE	SINM	AACE	IWRI	ETA (s)	MAXTE	AAXTE	SINM	AACE	IWRI	ETA (s)
Straight channel	Up	1.393	1.244	0	**161.242**	8.097	600	**0.854**	**0.292**	0	9.53x10^4	**0.515**	**586**
	Down	3.609	3.019	0.424	**920.526**	21.268	600	**3.494**	**2.438**	**0.312**	4.85x10^5	**17.132**	**578.5**
T-junction	Up	13.634	5.455	0.736	2.30x10^5	2.255	630	**9.319**	**3.112**	**0.335**	**1.24x10^5**	**0.607**	**529.5**
	Down	22.031	9.497	1.539	2.28x10^5	5.251	497	**7.148**	**1.731**	**0.056**	**1.40x10^5**	**-0.039**	**470.5**
	Up	**24.747**	4.873	0.670	**63.795**	1.625	1396	25.162	**3.737**	**0.461**	8.25x10^4	**0.747**	**1332.5**

River bend	Down	**25.358**	7.278	1.140	**124.01**	3.294	900.5	26.407	**5.160**	**0.794**	2.38×10^5	**1.884**	**857**

4.7. Discussion on the impact of static obstacles

In addition to its path-following capabilities, the NMPC can also aid in improving the vessel's collision-avoidance capabilities. Consider static obstacles such as buoys, a standstill vessel, or a permanent fixture. These obstacles can be incorporated into the planned path or detected in real-time, allowing the guidance system to update the vessel's trajectory dynamically. The following simulations consider manually modifying the waypoints without employing a collision avoidance algorithm. Preliminary results, as shown in Figure 25 visualize the resulting path followed by the IWV with a static obstacle along its route. The obstacle is located at the coordinates $(1000,435)$, having a length and width equal to 30 m and 15 m, respectively. The NMPC is capable of handling the sharp change in the reference trajectory by effectively mitigating cross-track errors without leading to instability. On the other hand, the PID controller takes a longer time to steer the vessel back towards the reference trajectory. Furthermore, it avoids the static obstacle with only a small margin. This again emphasises the advantage of employing predictive control, which is crucial for scenarios involving sharp turns. To further enhance the tracking performance, a variable speed control may be employed in this case.

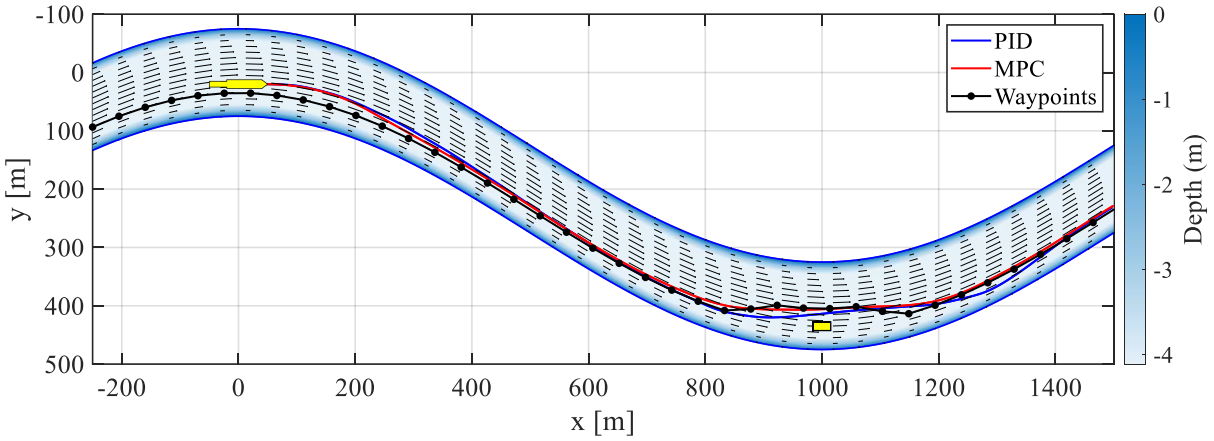

Figure 25. Trajectories in the river bend with a static obstacle (x=1000 m).

4.8. Comparison of NMPC's performance against a linearised MPC

On a reviewer's suggestion, in this subsection, we provide further justification for using NMPC instead of a Linearised MPC (LMPC). Firstly, the LMPC implementation is carried out using a Nomoto (KT) manoeuvring model (Nomoto et al., 1957). This model simplifies the vessel's motions into its turning and course-keeping capability, represented by second-order linear dynamics and is a popular choice for vessel heading control (He et al., 2023). The linearisation is performed by using a multi-equilibrium point approach, where the vessel's nonlinear equations of motion are locally linearised around a sequence of equilibrium/reference heading angles (ψ^{ref}), yaw rates (r^{ref}) and rudder angles (δ^{ref}). Since the model is re-linearised at each time step, it is more accurate as compared to a single global linearisation approach. The resulting model can be expressed as

$$\delta\bar{q}(k+1) = A(k)\delta\bar{q}(k) + B(k)\delta\bar{p}(k) \tag{40}$$

where, $\delta\bar{q} = \bar{q} - \bar{q}^{\mathrm{ref}}$, $\delta p = \bar{p} - \bar{p}^{\mathrm{ref}}$ represent small deviations of the vessel states and control inputs from the reference values, with $q^{\mathrm{ref}} = \left[\ \psi^{\mathrm{ref}}\ r^{\mathrm{ref}}\ \dot{r}^{\mathrm{ref}}\ \right]^T$ and $p^{\mathrm{ref}} = \left[\ \delta^{\mathrm{ref}}\ \dot{\delta}^{\mathrm{ref}}\ \right]^T$. $A(k)$ and $B(k)$ are the state and input matrices, respectively, derived from the Jacobian of the original nonlinear system at the current reference point. The resulting LMPC then solves a quadratic OCP at each time interval, using the updated linear model and reference values.

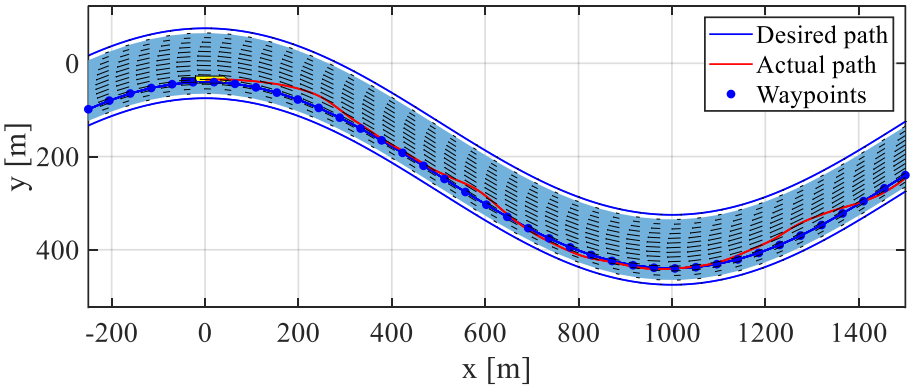

(a) Trajectory for upstream sailing.

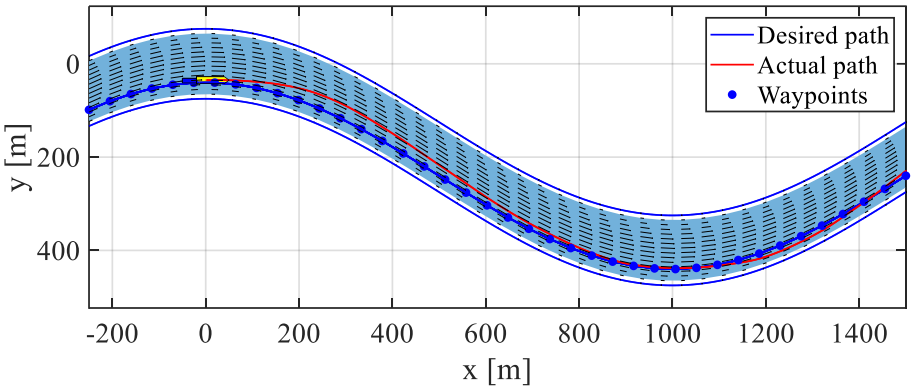

(b) Trajectory of downstream sailing.

Figure 26. Trajectories of control simulations on river bends with LMPC.

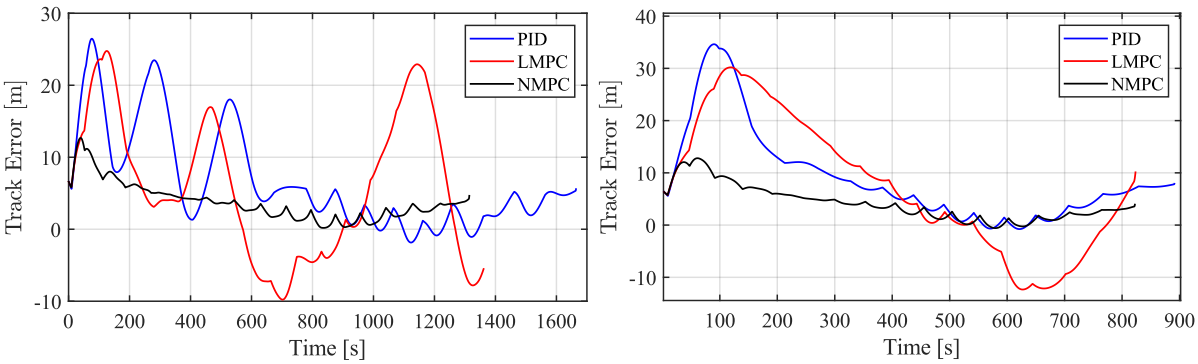

(a) SXTE (Upstream case). (b) SXTE (Downstream case).

Figure 27. Signed cross-track error comparison with LMPC for the upstream and downstream sailing cases.

Table 6. The values of the key performance metrics for the different controllers in river bends scenario. The minimum values obtained for each metric are highlighted in bold.

	Current stream	MAXTE	AAXTE	SINM	AACE	IWRI	ETA (s)
LMPC	Up	24.759	9.357	1.625	404.908	4.933	1362
	Down	30.194	11.769	1.962	278.577	6.358	**823.5**
PID	Up	**24.747**	4.873	0.670	**63.795**	1.625	1396
	Down	**25.358**	7.278	1.140	**124.01**	3.294	900.5
NMPC	Up	25.162	**3.737**	**0.461**	8.25×10^4	**0.747**	**1332.5**
	Down	26.407	**5.160**	**0.794**	2.38×10^5	**1.884**	857

The river bends scenario, as previously described in Section 4.5 is simulated for a canal with a bottom width of W_{CB}=120m. The control objective is to steer the vessel towards a predefined route at a lateral distance of 35 m from the bank and follow the path. The vessel's resulting trajectories for upstream and downstream sailing are shown in Figure 26(a) and (b), respectively. Further, the signed cross-track errors are visualised in Figure 27(a) and (b), compared against the PID controller and NMPC. It can be observed that LMPC has inferior tracking performance to both controllers as the overall XTE is significantly higher. This relatively inferior performance of LMPC can be attributed to the widely varying operating conditions due to bank forces and current direction in the bends. As described in Equations (2) and (13), the forces acting on the vessel hull and the bank-induced forces are highly nonlinear in the vessel's states. Even with the multi-equilibrium linearisation approach, significant model mismatch is observed, which increases with the increase in prediction horizon, leading to higher tracking errors. On the other hand, the PID controller does not face this limitation.

On the key performance metrics (see Table 6), LMPC has a comparable performance with the PID controller and NMPC for the MAXTE and ETA metrics. However, it performs poorly on the AAXTE, SINM and IWRI metrics. On the AACE metric, it performs significantly better than NMPC but is not as effective as the PID controller. Overall, it is evident that the current implementation of LMPC can be further improved for effective path planning control under different conditions. Various modifications have been proposed in the literature to improve its performance, such as disturbance estimation (Abdelaal et al., 2018; Zhang et al., 2017), state-compensated extended state observers (Liu et al., 2017a), etc.

5. Conclusions

This paper focuses on the modelling, design and analysis of an improved model-predictive heading control method for the path following of inland waterway vessels. The rigid body dynamics of the vessel are calculated based on a modified MMG model incorporating specific hydrodynamic impacts of inland water, including shallow water, river current and bank effects. The performance of the proposed NMPC is firstly evaluated against the standard PID controller based on the cross-track error and control efforts metrics under various inland waterway scenarios. Additionally, key performance metrics are proposed for evaluating the control performance based on navigation requirements specific to inland waterways.

The simulation was first conducted in straight channel conditions, with the objective of maintaining the vessel's path at a specific vessel-bank distance. The simulation shows that both PID and NMPC have good tracking performance under both current directions, with NMPC exhibiting smaller tracking errors and fewer rudder efforts, particularly during the downstream sailing condition.

Unlike straight-channel sailing, vessel path control in confluences is significantly more complex due to the difficulties in handling the vessel during tight manoeuvres under limited turning space. To validate the control performance and feasibility under these conditions, a sharp turning at a waterway confluence was simulated. The proposed NMPC demonstrates superior results under this challenging scenario, where the tracking error can be reduced within 5 m. On the other hand, the PID controller has a much larger course deviation, and the error exceeds more than 20 m during turning. The simulation results conclude that the NMPC can effectively optimise the rudder control actions based on the vessel's future behaviour to prevent frequent turning or large deflections.

Lastly, the simulation was conducted considering river bends, and the impact of propulsion speeds and bank geometries at different bank slopes was evaluated. Interestingly, increasing the vessel's speed reduces the tracking error in the NMPC case, yet leads to the opposite behaviour in the PID controller's case. This is because increasing speed shortens the vessel's reaction time for the PID controller, even though the rudder steering force increases at higher propulsion speeds. In contrast, NMPC can anticipate the vessel's future behaviour and optimally allocate control input.

The decreasing waterway bottom width significantly impacts the PID controller's performance since the vessel is subject to a stronger bank effect due to higher constraint levels. On the contrary, NMPC showed minor disturbances and demonstrated good tracking performance. The performance of NMPC was also found to be significantly better than the PID controller on the proposed key performance metrics. A smaller value of MAXTE, AAXTE and SINM metrics indicates a superior control performance of the NMPC, whereas a small IWRI indicates its higher robustness in comparison to the PID controller. In addition, it achieves a comparatively smaller ETA, which further establishes its applicability for inland navigation. A sharp changing reference trajectory resulting from a collision avoidance scenario is also simulated, where, unlike the PID controller, the NMPC can maintain an acceptable error margin and avoid unstable manoeuvres. Finally, a comparison is made between the NMPC and its linear counterpart, LMPC. While LMPC is preferred for its simplicity and faster computation, simpler linear models do not provide sufficient robustness against environmental disturbances. LMPC in conjunction with state estimation and disturbance mitigation-based methods may improve control performance.

Future research will focus on improving the robustness of the MPC in the presence of parameter uncertainties and unmodelled dynamics. Here, incorporating data-driven techniques can be particularly useful. Furthermore, variable speed control could further enhance the controller's performance, allowing for more responsive adjustments to changing navigation conditions.

Acknowledgements

This project has received funding from the European Union's EU Framework Programme for Research and Innovation Horizon 2020 under Grant Agreement No. 955768 (ETN AutoBarge). Project website: https://etn-autobarge.eu/.

References

Abdelaal, M., Fränzle, M., Hahn, A., 2018. Nonlinear Model Predictive Control for trajectory tracking and collision avoidance of underactuated vessels with disturbances. Ocean Engineering 160, 168-180.
Abkowitz, M.A., 1964. Lectures on ship hydrodynamics--Steering and manoeuvrability.
Alessandri, A., Donnarumma, S., Vignolo, S., Figari, M., Martelli, M., Chiti, R., Sebastiani, L., 2015. System control design of autopilot and speed pilot for a patrol vessel by using LMIs. Towards Green Marine Technology and Transport, 577-583.
Andersson, J.A.E., Gillis, J., Horn, G., Rawlings, J.B., Diehl, M., 2019. CasADi: a software framework for nonlinear optimization and optimal control. Math Program Comput 11 (1), 1-36.
Bakaric, V., Vukic, Z., Antonic, R., 2004. Improved basic planar algorithm of vehicle guidance through waypoints by the line of sight, First International Symposium on Control, Communications and Signal Processing, 2004. IEEE, pp. 541-544.
BBC News, 2021. Suez Canal: Owner of cargo ship blocking waterway apologises.
Breivik, M., Fossen, T.I., 2008. Guidance Laws for Planar Motion Control. Ieee Decis Contr P, 570-577.
Chen, C., Delefortrie, G., Lataire, E., 2021. Effects of water depth and speed on ship motion control from medium deep to very shallow water. Ocean Engineering 231.
Chen, Y.-H., Ellis-Tiew, M.-Z., Chan, Y.-H., Lin, G.-W., Chen, Y.-Y., 2023. Trajectory Tracking Design for Unmanned Surface Vessels: Robust Control Approach. Journal of Marine Science and Engineering 11 (8).
Du, P., Ouahsine, A., Sergent, P., Hu, H., 2020. Resistance and wave characterizations of inland vessels in the fully-confined waterway. Ocean Engineering 210, 107580.
Du, Z., Negenborn, R.R., Reppa, V., 2022a. COLREGS-Compliant collision avoidance for physically coupled multi-vessel systems with distributed MPC. Ocean Engineering 260.
Du, Z., Negenborn, R.R., Reppa, V., 2022b. Multi-Objective Cooperative Control for a Ship-Towing System in Congested Water Traffic Environments. Ieee T Intell Transp 23 (12), 24318-24329.
European Commission, 2020. MSCA-ETN-AUTOBarge.
European Commission, 2023. Freight transport statistics - modal split.
Fossen, T.I., Breivik, M., Skjetne, R., 2003. Line-of-sight path following of underactuated marine craft. IFAC proceedings volumes 36 (21), 211-216.
Fossen, T.I., Lekkas, A.M., 2017. Direct and indirect adaptive integral line-of-sight path-following controllers for marine craft exposed to ocean currents. Int J Adapt Control 31 (4), 445-463.
Friedhoff, B., Hoyer, K., List, S., Tenzer, M., 2019. Investigation of the nominal and effective propeller inflow for a family of inland waterway vessels. Ocean Engineering 187.
Fu, H., Yao, W., Cajo, R., Zhao, S., 2023. Trajectory Tracking Predictive Control for Unmanned Surface Vehicles with Improved Nonlinear Disturbance Observer. Journal of Marine Science and Engineering 11 (10).
Gros, S., Zanon, M., Quirynen, R., Bemporad, A., Diehl, M., 2020. From linear to nonlinear MPC: bridging the gap via the real-time iteration. Int J Control 93 (1), 62-80.
Hart, F., Okhrin, O., Treiber, M., 2023. Vessel-following model for inland waterways based on deep reinforcement learning. Ocean Engineering 281.
Haseltalab, A., Negenborn, R.R., 2019. Model predictive maneuvering control and energy management for all-electric autonomous ships. Appl Energ 251.
He, H.W., Van Zwijnsvoorde, T., Lataire, E., Delefortrie, G., 2023. Model predictive controller for path following ships validated by experimental model tests. Ocean Engineering 288.
Kaidi, S., Smaoui, H., Sergent, P., 2017. Numerical estimation of bank-propeller-hull interaction effect on ship manoeuvring using CFD method. Journal of Hydrodynamics, Ser. B 29 (1), 154-167.
Kayacan, E., Park, S., Ratti, C., Rus, D., 2019. Learning-based Nonlinear Model Predictive Control of Reconfigurable Autonomous Robotic Boats: Roboats. Ieee Int C Int Robot, 8230-8237.
Kijima, K., Nakiri, Y., 1990. Prediction method of ship manoeuvrability in deep and shallow waters.
Kim, D., Tezdogan, T., Incecik, A., 2022. Hydrodynamic analysis of ship manoeuvrability in shallow water using high-fidelity URANS computations. Applied Ocean Research 123, 103176.
Kirches, C., Wirsching, L., Bock, H.G., Schlöder, J.P., 2012. Efficient direct multiple shooting for nonlinear model predictive control on long horizons. J Process Contr 22 (3), 540-550.

Koh, K., Yasukawa, H., 2012. Comparison study of a pusher–barge system in shallow water, medium shallow water and deep water conditions. Ocean engineering 46, 9-17.
Kosch, M., Elkhashap, A., Koschorrek, P., Zweigel, R., Abel, D., 2021. Hardware-in-the-Loop Trajectory Tracking and Collision Avoidance of Automated Inland Vessels Using Model Predictive Control. 2021 European Control Conference (Ecc), 2251-2256.
Lee, C.-K., Lee, S.-G., 2008. Investigation of ship maneuvering with hydrodynamic effects between ship and bank. Journal of Mechanical Science and Technology 22, 1230-1236.
Li, S., Liu, J., Negenborn, R.R., Wu, Q., 2020. Automatic Docking for Underactuated Ships Based on Multi-Objective Nonlinear Model Predictive Control. IEEE Access 8, 70044-70057.
Liu, C.G., Negenborn, R.R., Zheng, H.R., Chu, X.M., 2017a. A state-compensation extended state observer for model predictive control. Eur J Control 36, 1-9.
Liu, J., Hekkenberg, R., Quadvlieg, F., Hopman, H., Zhao, B., 2017b. An integrated empirical manoeuvring model for inland vessels. Ocean Engineering 137, 287-308.
Liu, J., Hekkenberg, R., Rotteveel, E., Hopman, H., 2015. Literature review on evaluation and prediction methods of inland vessel manoeuvrability. Ocean Engineering 106, 458-471.
Mucha, P., 2017. On simulation-based ship maneuvering prediction in deep and shallow water. Dissertation, Duisburg, Essen, Universität Duisburg-Essen, 2017.
Mucha, P., Dettmann, T., Ferrari, V., el Moctar, O., 2019. Experimental investigation of free-running ship manoeuvers under extreme shallow water conditions. Applied Ocean Research 83, 155-162.
Naeem, W., Sutton, R., Ahmad, S., Burns, R., 2003. A review of guidance laws applicable to unmanned underwater vehicles. the Journal of Navigation 56 (1), 15-29.
Nomoto, K., Taguchi, T., Honda, K., Hirano, S., 1957. On the steering qualities of ships. International Shipbuilding Progress 4 (35), 354-370.
Ogawa, A., Kasai, H., 1978. On the mathematical model of manoeuvring motion of ships. International shipbuilding progress 25 (292), 306-319.
Okuda, R., Yasukawa, H., Sano, M., Hirata, N., Yoshimura, Y., Furukawa, Y., Matsuda, A., 2022. Maneuvering simulations of twin-propeller and twin-rudder ship in shallow water using equivalent single rudder model. Journal of Marine Science and Technology 27 (2), 948-970.
Park, B.S., Kwon, J.-W., Kim, H., 2017. Neural network-based output feedback control for reference tracking of underactuated surface vessels. Automatica 77, 353-359.
Paulig, N., Okhrin, O., 2024. Robust path following on rivers using bootstrapped reinforcement learning. Ocean Engineering 298.
Pompée, P.-J., 2015. About modelling inland vessels resistance and propulsion and interaction vessel-waterway key parameters driving restricted/shallow water effects. Proceeding of Smart Rivers 2015.
Sano, M., Yasukawa, H., Hata, H., 2014. Directional stability of a ship in close proximity to channel wall. Journal of Marine Science and Technology 19 (4), 376-393.
Saravanakumar, S., Asokan, T., 2011. Waypoint Guidance based Planar Path Following and Obstacle Avoidance of Autonomous Underwater Vehicle, ICINCO (2), pp. 191-198.
Sun, T., Zhang, J., Pan, Y., 2017. Active DIsturbance Rejection Control of Surface Vessels Using Composite Error Updated Extended State Observer. Asian Journal of Control 19 (5), 1802-1811.
Tondel, P., Johansen, T.A., Bemporad, A., 2003. An algorithm for multi-parameffic quadratic programming and explicit MPC solutions. Automatica 39 (3), 489-497.
Vantorre, M., Delefortrie, G., Eloot, K., Laforce, E., 2003. Experimental investigation of ship-bank interaction forces.
Wachter, A., Biegler, L.T., 2006. On the implementation of an interior-point filter line-search algorithm for large-scale nonlinear programming. Math Program 106 (1), 25-57.
Waltz, M., Paulig, N., Okhrin, O., 2025. 2-level reinforcement learning for ships on inland waterways: Path planning and following. Expert Syst Appl 274.
Wang, L., Wu, Q., Liu, J., Li, S., Negenborn, R., 2019. State-of-the-Art Research on Motion Control of Maritime Autonomous Surface Ships. Journal of Marine Science and Engineering 7 (12).
Wei, H., Zhao, Y., Changyin, S., 2017. Adaptive Neural Network Control of a Marine Vessel With Constraints Using the Asymmetric Barrier Lyapunov Function. IEEE Trans Cybern 47 (7), 1641-1651.
Xu, D., Huang, Y., Zhou, X., Xu, H., 2023. Path following control for large inland ships in a restricted waterway using the nonlinear terminal sliding mode method. Ocean Engineering 284.

Yan, X., Wang, K., Yuan, Y., Jiang, X., Negenborn, R.R., 2018. Energy-efficient shipping: An application of big data analysis for optimizing engine speed of inland ships considering multiple environmental factors. Ocean Engineering 169, 457-468.
Yang, Y., el Moctar, O., 2024. A mathematical model for ships maneuvering in deep and shallow waters. Ocean Engineering 295, 116927.
Yasukawa, H., Yoshimura, Y., 2015. Introduction of MMG standard method for ship maneuvering predictions. Journal of marine science and technology 20, 37-52.
Yoshimura, Y., 1986. Mathematical model for the manoeuvring ship motion in shallow water. Journal of the Kansai society of naval architects (200).
Zhang, C., Dhyani, A., Ringsberg, J.W., Thies, F., Reppa, V., Negenborn, R.R., 2024a. Manoeuvring Modelling and Control Design of Autonomous Vessels on Inland Waterways, 43rd International Conference on Offshore Mechanics and Arctic Engineering. American Society of Mechanical Engineers.
Zhang, C., Ma, Y., Thies, F., Ringsberg, J.W., Xing, Y., 2024b. Towards autonomous inland shipping: a manoeuvring model in confined waterways. Ships and Offshore Structures, 1-13.
Zhang, C., Ringsberg, J.W., Thies, F., 2023. Development of a ship performance model for power estimation of inland waterway vessels. Ocean Engineering 287, 115731.
Zhang, J., Sun, T., Liu, Z., 2017. Robust model predictive control for path-following of underactuated surface vessels with roll constraints. Ocean Engineering 143, 125-132.
Zhang, J., Yu, S., Wu, D., Yan, Y., 2020a. Nonsingular fixed-time terminal sliding mode trajectory tracking control for marine surface vessels with anti-disturbances. Ocean Engineering 217.
Zhang, Q., Ding, Z.Y., Zhang, M.J., 2020b. Adaptive Self-Regulation Pid Control of Course-Keeping for Ships. Pol Marit Res 27 (1), 39-45.
Zheng, H., Negenborn, R.R., Lodewijks, G., 2014. Trajectory tracking of autonomous vessels using model predictive control, 19th IFAC World Congress.
Zheng, H., Negenborn, R.R., Lodewijks, G., 2016. Predictive path following with arrival time awareness for waterborne AGVs. Transportation Research Part C: Emerging Technologies 70, 214-237.
Ziegler, J.G., Nichols, N.B., 1942. Optimum settings for automatic controllers. Transactions of the American society of mechanical engineers 64 (8), 759-765.